

# Sentinel Lymph Node Staging and Detection in Melanoma Patients; Implementation of the MelaDiff Trial

Iris Marlou Huinink

Technical Medicine  
August 30, 2024

## **Committee**

Prof. dr. ir. B. Ten Haken

dr. A.E. Dassen

dr. ir. L. Alic

dr. A. Christenhusz

R. Lambers MSc

dr. B. Wermelink

# Contents

<b>1</b>	<b>Introduction</b>	<b>2</b>
<b>2</b>	<b>Background</b>	<b>6</b>
2.1	Principals of Differential Magnetometry (DiffMag handheld probe)	6
2.2	Compressed Sensing in MRI	7
2.3	Current ex vivo LN MRI protocol	8
<b>3</b>	<b>Method</b>	<b>10</b>
3.1	In vivo evaluation of the DiffMag handheld probe	10
3.2	Optimization of the ex vivo LN MRI protocol with Compressed Sensing	11
3.2.1	Compressed Sensing in T1- and T2-Weighted Fast Spin Echo MRI	12
3.2.2	Regularization parameter	13
3.2.3	Image quality assessment	13
3.2.4	Compressed Sensing in MRI maps	14
<b>4</b>	<b>Results</b>	<b>15</b>
4.1	In vivo evaluation of the DiffMag handheld probe	15
4.2	Optimization of the ex vivo LN MRI protocol with Compressed Sensing	15
4.2.1	Compressed Sensing in T1- and T2-Weighted Fast Spin Echo MRI	15
4.2.2	Compressed Sensing in MRI maps	18
<b>5</b>	<b>Discussion</b>	<b>21</b>
<b>6</b>	<b>Conclusion</b>	<b>25</b>
<b>A</b>	<b>MelaDiff trial</b>	<b>28</b>
A.1	Summary MelaDiff protocol	28
A.2	Approval MEC-U	29
A.3	Approval 'lokale uitvoerbaarheid' ZGT	30
<b>B</b>	<b>Lymphatic system of pigs</b>	<b>31</b>
<b>C</b>	<b>Questionary usability DiffMag handheld probe</b>	<b>32</b>

# 1 Introduction

Approximately 8,000 individuals are diagnosed with melanoma each year in the Netherlands[1]. The incidence of melanoma has steadily increased over the past 40 years, largely due to excessive childhood sun exposure and, to a smaller extent, artificial UV sources like tanning beds. Based on current trends, an increase in melanoma incidence in the Netherlands is expected in the coming years[2]. Melanoma is a highly aggressive form of skin cancer originating from malignant melanocytes. The primary risk factor for developing melanoma is exposure to natural or artificial ultraviolet (UV) rays which are known for their genotoxic effects[3]. Additional risk factors include the number of melanocytic nevi, family history, and genetic susceptibility. Melanoma is characterized by its high propensity to metastasize and metastases may appear years after the initial tumor treatment[4]. Patients diagnosed with metastatic melanoma at a later stage face poor prospects, as the disease becomes increasingly challenging to cure.

The current therapeutic approach for melanoma patients diagnosed after a diagnostic excision with a melanoma stage pT1b or higher(TNM8)—indicating melanomas with a thickness of less than 0.8 mm with ulceration or more than 1 mm, with or without ulceration—involves performing a surgical re-excision of the scar and assessing the nodal status with a Sentinel Lymph Node Biopsy(SLNB)[2]. A SLNB offers a precise evaluation of the disease stage, as melanoma staging is determined by the extent and spread of the cancer. Consequently, the presence of metastatic cells in regional lymph nodes (LNs) upstages a patient from stage I or II(regional disease) to stage III(metastasis in regional LNs). For this reason, the presence of metastatic cells in regional LNs is considered the most important prognostic indicator for disease-free survival and serves as a guide for possible adjuvant therapy[2]. While research shows varying results for these adjuvant therapy in melanoma stages II and III regarding disease-free survival[2], increasingly promising outcomes are emerging recently[5, 6]. As a result, accurate staging with SLNB is becoming even more critical to prevent patients from over- and undertreatment with these aggressive therapies[7, 8].

In the current standard of care for SLNB, a tracer (radioactive substance and/or blue dye) is injected near the scar at the primary tumor location. The tracer travels through the lymphatic system to the sentinel lymph node (SLN). The SLN is the first LN in the direct drainage pathway from the primary tumor to the regional nodal basin. This allows visualization of SLNs by preoperative lymphoscintigraphy and makes SLNs intraoperatively detectable using a gamma probe. This is followed by surgical dissection and evaluation of the LN(s) at the histopathology department. This method accurately identifies the LN most likely to contain metastases from the primary tumor and accurately detects the presence of metastatic cells with pathological examination. However, this technique has several drawbacks, including radiation exposure for both patients and healthcare personnel, stringent legislative controls, the decay of radiotracers, limited availability of radiotracers, and reliance on nuclear medicine units[9]. Furthermore, the SLNB procedure itself can lead to complications as lymphedema, reduced strength, and pain in patients[10]. These factors demonstrate a clinical need for a new, radiation-free, method for accurate SLN localization and staging.

To address the limitations of the radioactive tracer, a magnetic SLNB using Super Paramagnetic Iron-Oxide (SPIO) nanoparticles was developed[11]. In this procedure, SPIO particles are injected near the primary tumor site. Similar to the radioactive method, the SPIOs travel through the lymphatic system, enabling the detection of the SLN(s) using a magnetic probe. This offers numerous benefits such as no radiation exposure, easy accessibility of the tracer and a long shelf life. However, the currently available magnetometer for intraoperative detection of SPIO-enhanced LNs faces challenges which include a relatively low detection depth, biological noise, and interference from surgical equipment. Therefore, surgeons need to switch to plastic or carbon tools, and the system needs to be balanced prior to each measurement, which increases surgery time. To overcome these issues, the MD&I group at the University of Twente (UT) developed a differential magnetometry (DiffMag handheld probe) technique. This patented detection principle utilizes the nonlinear magnetic SPIO response and is therefore unaffected by surgical equipment[12, 13].

An additional advantage of SPIOs is their visibility on Magnetic Resonance Imaging (MRI). This visibility allows for SPIOs to be used as contrast agent, which offers the potential for preoperative staging and mapping[14]. Identifying the SLN in melanoma patients with unclear drainage patterns, such as those with tumors on the abdomen or back, can be challenging. This makes the radioactive preoperative lymphoscintigraphy crucial. To overcome this and eliminate the need for radioactivity, SPIO-enhanced mapping with MRI is explored as a potential replacement for this preoperative lymphoscintigraphy[15, 16]. Additionally, studies also explore a non-invasive method for accurately staging LNs using this SPIO enhanced MRI. Previous research revealed that the intravenous injection of SPIOs could enhance MRI to non-invasively predict the nodal status of patients with prostate cancer[17]. This enhancement stemmed from the absorption of SPIO-particles by macrophages gathering in LNs, making them noticeably dark on MRI images. However, in regions where malignancy affects

the LNs and macrophage accumulation does not occur, the LNs maintain their original intensity on MRI images. Therefore, the uneven distribution of iron within the SLN can serve as a valuable indicator of the presence of metastasis in the SLN[18, 14].

The combination of the DiffMag handheld probe and the mapping and staging with SPIO-enhanced MRI holds promise for a new, radiation-free, and for some patients, non-invasive approach to SLN detection and evaluation. In this approach all patients receive a SPIO injection, followed by an MRI scan to non-invasively assess the nodal status. If staging is accurate, an SLNB is unnecessary, and only a re-excision is required. If there is any doubt in the evaluation, a Magnetic SLNB using the DiffMag handheld probe is performed during the same procedure as the tumor site re-excision. This approach spares many patients from the potential complications of a SLNB procedure.

The feasibility of the DiffMag handheld probe and SPIO-enhanced MRI staging are not yet proven. To address these aspects, the MelaDiff trial was initiated. This trial is a multi-centre clinical trial detailed in Appendix A.1. It utilises SPIO-enhanced preoperative MRI, perioperative LN identification using DiffMag and postoperative MRI staging. In this trial the DiffMag handheld probe is evaluated and the possibility of non-invasively staging LNs with SPIO-enhanced MRI is further explored. Figure 1.2 gives an overview of the current standard of care SLNB, the steps of the MelaDiff trial and the ideal magnetic procedure as written above.

Before the trial can be implemented, it faces two challenges. Figure 1.2 shows two red circles, indicating the locations in the trial of these challenges. The first challenge is that the DiffMag handheld probe has never been used in vivo, meaning no prior experience exists in a clinical setting. As a result, it is unclear what issues might arise during the trial or if any optimizations are necessary before its evaluation in melanoma patient care. The second challenge lies in the MRI data acquisition process, which is notably time-consuming. The MelaDiff trial first focuses on ex vivo MRI as this offers higher image resolution and allows for a closer examination of the SPIO distribution patterns in both healthy and metastatic LN tissue[14]. Multiple sequences are scanned during this imaging process to identify the most optimal sequence for LN staging. Figure 1.1 presents ex vivo MRI images obtained in previous research of two healthy LNs and one metastatic LN, along with their corresponding pathological slices. These images are of high quality and allow for a good assessment of the SPIO distribution.

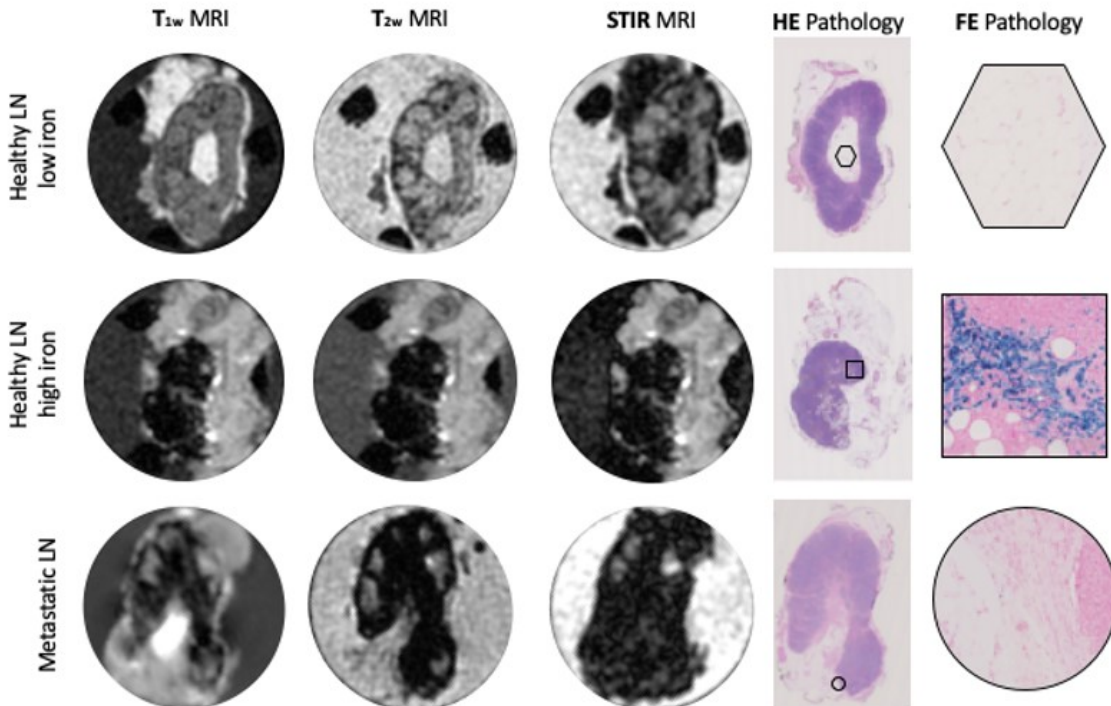


Figure 1.1: MRI and corresponding pathology images obtained in LowMag trial for a low iron-content LN (first row), a high iron-content LN (second row) and metastatic LN with high iron-content[14].

However, the need for this high quality images and the use of multiple sequences result in an average scan time of approximately 340 minutes( $\approx 6$  hours) per LN. This lengthy acquisition time limits its clinical applicability, as this duration is unfeasible for routine use in daily clinical practice. Additionally, it hinders research

efficiency and restricts the integration of newly developed sequences during research. To address these issues, Compressed Sensing (CS) has been proposed as a method to accelerate the image acquisition process[19]. In MRI, CS has the potential to substantially reduce acquisition time while preserving image quality[20]. Previous work has applied CS on the ex vivo MRI scanner[19]. However, it did not integrate CS into T2-weighted images and MRI maps, and only utilized standardized parameters. For this reason, this thesis concentrates on evaluating the performance of the DiffMag handheld probe in vivo and integrating and evaluating CS in the ex vivo MRI LN protocol. This research is guided by the following questions:

**Primary research question:**

How can the implementation of the MelaDiff trial be optimized to achieve a radiation free, potentially non-invasive way of sentinel lymph node staging and detection in melanoma patients using differential magnetometry (DiffMag) and SPIO-enhanced MRI?

**Secondary research questions:**

1. How does the in vivo usability and feasibility of the DiffMag handheld probe compare to that of the SentiMag?
2. To what extent can T1/T2 weighted images and T1/T2 maps be accelerated with CS while maintaining acceptable image quality?

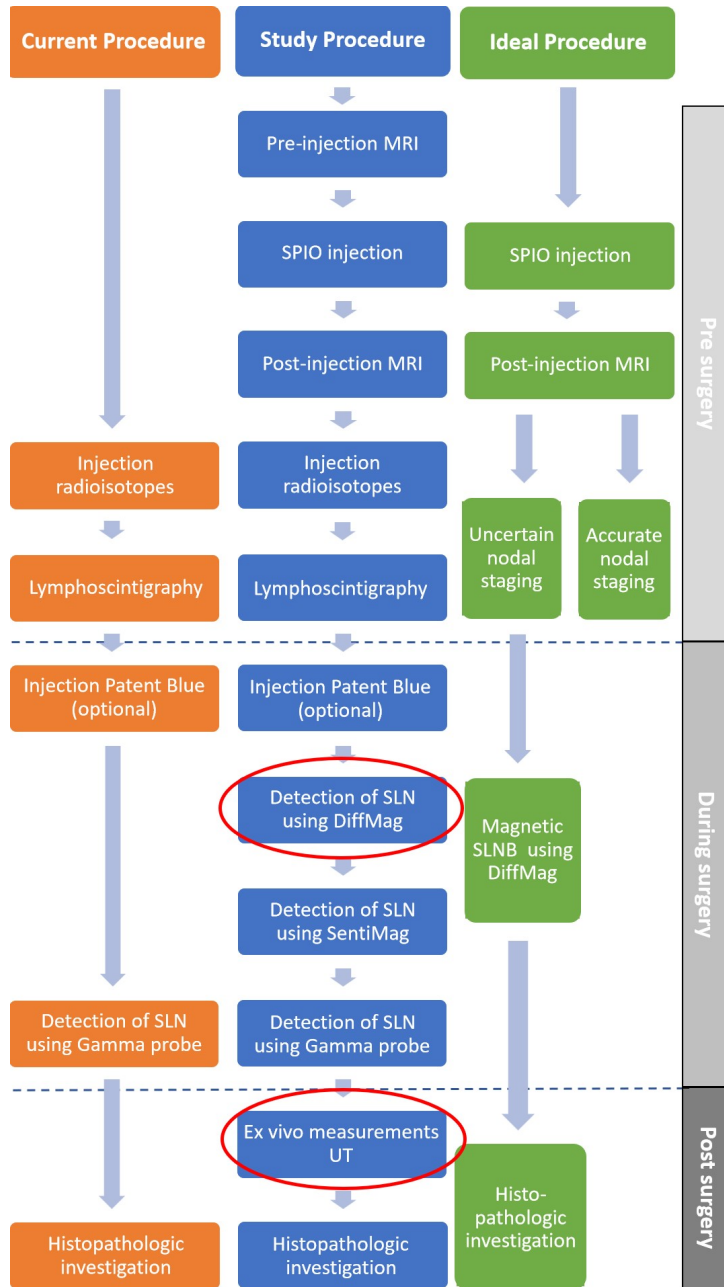


Figure 1.2: Overview of the current standard of care SLNB, the MelaDiff trial and the ideal procedure. For the conventional SLNB procedure (orange blocks), a radioactive tracer is injected at the primary tumor site at a maximum of 24 hours before surgery. Lymphoscintigraphy is used to localize the SLNs preoperatively. According to the local protocol, a blue dye is injected preoperatively, which can visually guide the surgeon to the SLNs. The SLNs are intraoperatively detected using the blue discoloration and the radioactivity measured by the gamma probe. Investigation of the SLNs at the department of histopathology indicate if metastases are present. In the MelaDiff trial (blue blocks) the magnetic procedure will be studied in addition to the current procedure to compare the magnetic SLNB to the gold standard. Moreover, the DiffMag device will be compared to the CE-marked SentiMag. For magnetic SLNB procedure, SPIO particles are injected at the primary tumor site additionally to the radioactive injection. Preoperative MRI will be used for SLN localization. The SLNB will be performed using the SentiMag, DiffMag and gammaprobe. Investigation of the SLNs at the department of histopathology indicate if metastases are present. The red circles indicate at which parts the MelaDiff trial is optimized in the current thesis. In the ideal procedure (green blocks) all patients receive a SPIO injection, followed by an MRI scan to non-invasively assess the nodal status. If staging is accurate, an SLNB is unnecessary, and only a re-excision is required. However, if there is any doubt in the evaluation, a Magnetic SLNB using the DiffMag handheld probe is performed.

## 2 Background

This thesis concentrates on evaluating and identifying problems of the DiffMag handheld probe, along with integrating and assessing CS in the ex vivo LN MRI imaging protocol. For this reason, the underlying principles of both techniques are explained, followed by an explanation of the current ex vivo LN MRI protocol.

### 2.1 Principals of Differential Magnetometry (DiffMag handheld probe)

The DiffMag detection principle uses the nonlinear magnetic SPIO response and should therefore be unaffected by surgical equipment[13]. To be unaffected by surgical equipment, it is crucial to isolate a signal specific to these of SPIO particles. The University of Twente observed such a signature in the nonlinear magnetization characteristics of the SPIOs[21]. This nonlinear characteristic differs from the linear magnetization behavior of predominantly diamagnetic tissues as surgical equipment. This principal is shown in Figure 2.1.

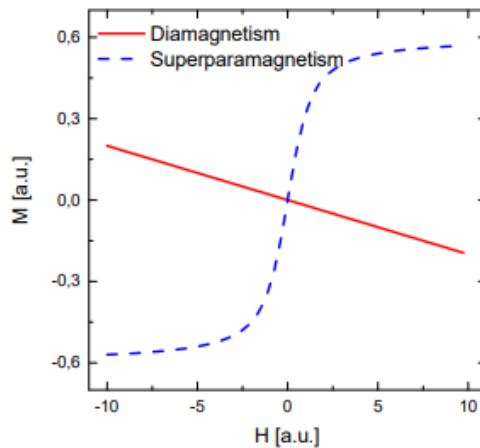


Figure 2.1: The signature of the nonlinear magnetization characteristics of nanoparticles (blue) and the linear magnetization behavior of predominantly diamagnetic tissues (red). The behavior of the nanoparticles clearly differs from that of other diamagnetic tissues, giving them a unique signature[22].

When a sample containing SPIOs is exposed to a small oscillating magnetic field, it can be detected as a voltage across the detection coil. This concept forms the foundation of conventional magnetometry, wherein the detection voltage is proportional to the derivative of the magnetization curve around zero. Differential Magnetometry is an extension of conventional magnetometry. It additionally exploits the nonlinear magnetization curve of SPIO nanoparticles, whereas the background signal remains linear (as depicted in Figure 2.1). By comparing the values of the derivative at different points along the magnetization curve, it becomes possible to apply a series of alternating offset fields with an amplitude to the sample and simultaneously examine the derivative of the magnetization curve. This alternating offset field is shown in figure 2.2. This procedure ensures the background-independent detection of SPIO nanoparticles[21].

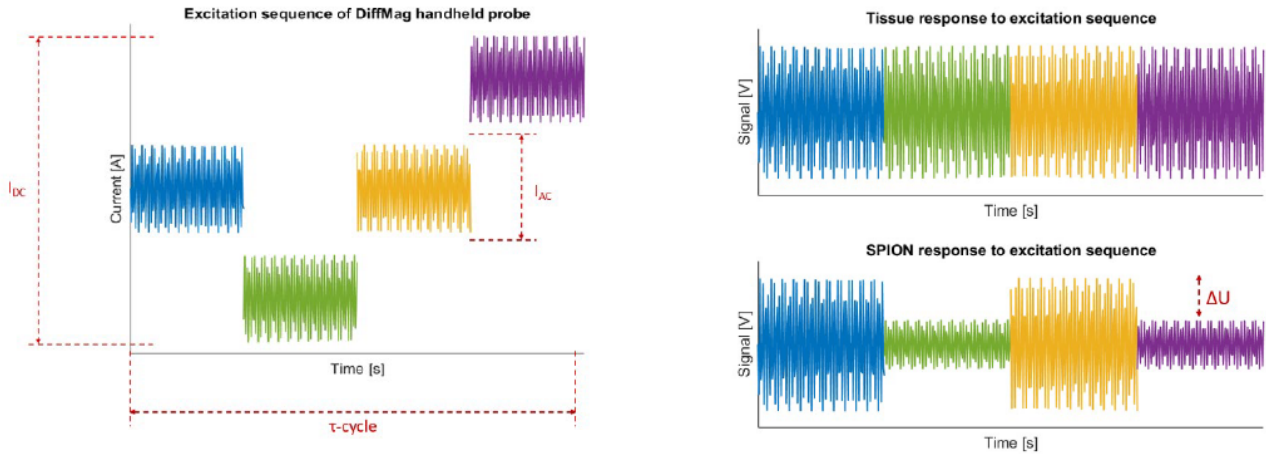


Figure 2.2: Left: Excitation sequence with no DC-offset field(blue), a negative DC-offset field (green), no DC-offset field (yellow) and a positive DC-offset field (purple). Right top: Resultant detector voltage of tissue without modulation. Right bottom: SPIOs with modulation

## 2.2 Compressed Sensing in MRI

MRI operates on the principle of aligning hydrogen nuclei in the body's tissues using a strong magnetic field[23]. When these nuclei are exposed to radiofrequency pulses, they emit signals that are used to create detailed images of internal structures.

One common MRI sequence used in *ex vivo* MRI protocol is Fast Spin Echo (FSE). FSE is a MRI imaging technique that acquires multiple echo signals in a single excitation[24]. It uses a series of refocusing pulses to quickly capture data, which significantly reduces scan times. In FSE sequences, the Turbo Factor plays a key role by defining the number of echoes collected per excitation. A higher Turbo Factor enables faster imaging by acquiring multiple echoes within each repetition time.

Besides the use of this faster sequence, CS also offers the potential to significantly speed up image acquisition while maintaining image quality[20]. Traditional MRI techniques acquire a large number k-space points to generate an image, resulting in relatively long scan times. K-space points represent the spatial frequency data collected during the scan, which are used to construct the final image. Each point in k-space corresponds to specific frequency and phase information that, when combined through a mathematical process called Fourier transformation, creates the detailed image of the scanned area. CS in MRI aims to reduce these number of samples needed to reconstruct an image, thus shortening scan times.

This smaller subset of k-space points is acquired using a random sampling pattern[25]. Sampling randomly is crucial because conventional equispaced undersampling followed by zero-filling leads to coherent aliasing. This means that the reconstructed image will contain superimposed replicas of the original signal. These exact replicas make it impossible to distinguish the original signal from and its replicas, as they are all equally alike (Figure 2.3c). Random undersampling presents a different scenario. An image with random undersampling will show incoherent artifact that look like random noise when a zero-filling fourier reconstruction is applied (Figure 2.3d).

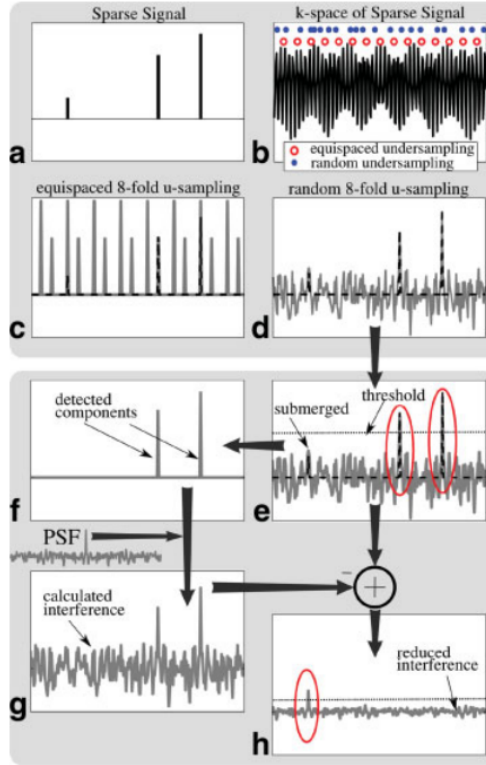


Figure 2.3: An intuitive reconstruction of a sparse signal from pseudo-random k-space undersampling. A sparse signal (a) is 8-fold undersampled in k-space (b). Equispaced undersampling results in coherent signal aliasing (c) that cannot be recovered. Pseudo-random undersampling results in incoherent aliasing (d). Strong signal components stick above the interference, are detected (e) and recovered (f) by thresholding. The interference of these components is computed (g) and subtracted (h), lowering the total interference level and enabling recovery of weaker components[20].

After acquiring this undersampled k-space data using random sampling patterns, the next step in CS MRI is the reconstruction of the image. The undersampled k-space data is converted to a spacial frequency domain using a WT. This results in a sparse signal (Figure 2.3e). In this way, the actual signal components become more prominent and distinguishable from noise and artifacts. This is because the sparse representation effectively highlights the important features of the image while suppressing noise and irrelevant details. After that, thresholding is employed to suppress the weaker signal components associated with noise and artifacts, leaving behind the stronger signal components corresponding to the actual image information (Figure 2.3f).

In reconstruction, the regularization parameter plays a crucial role in balancing the accuracy of the reconstruction and the sparsity of the signal[20]. Equation 1 describes the optimization process.

$$\min_x (\|y - Ax\|_2^2 + \lambda \|Wx\|_1) \quad (1)$$

An image  $x$  is sought that minimizes the given expression, which consists of two key components: a data accuracy term and a regularization term. The data accuracy term ensures that the reconstructed signal aligns with the acquired measurements, while the regularization term promotes sparsity within the solution space. In this context,  $x$  denotes the image, and  $y$  represents the acquired measurements. The sensing matrix  $A$  characterizes the measurement process, and  $W$  provides a sparse representation of the signal. The regularization parameter  $\lambda$  governs the trade-off between data accuracy and sparsity. A small  $\lambda$  favors accuracy but may compromise sparsity, whereas a large  $\lambda$  emphasizes sparsity at the cost of accuracy.

### 2.3 Current ex vivo LN MRI protocol

To identify the most optimal MRI sequence, or combination thereof, for SPIO-enhanced MRI LN staging, a wide range of sequences are included in research. The current ex vivo MRI protocol consists of T1- and T2-weighted FSE sequences, Short Tau Inversion Recovery (STIR) imaging, as well as T1- and T2-mapping.

Research has demonstrated that (U)SPIO-enhanced T1- and T2-Weighted MRI images can be used to non-invasively predict the nodal status[10, 26, 27]. T1-Weighted images highlight tissues based on their longitudinal

relaxation time (T1)[23]. In these images, fat and other tissues with shorter T1 times appear bright, while fluids, which have longer T1 times, appear darker. Conversely, T2-Weighted images emphasize the transverse relaxation time (T2), making fluids appear bright and tissues with shorter T2 times, like fat, appear darker. Echo Time (TE) is a crucial parameter in this process. It represents the time between the application of the radiofrequency pulse and the peak of the signal received from the tissue. TE affects the contrast in T2-Weighted images by determining how long the tissues have been allowed to dephase before the signal is captured. Similarly, Repetition Time (TR) is the interval between successive radiofrequency pulses applied to the same tissue slice. TR influences T1-Weighted image contrast by allowing tissues to relax between pulses, affecting their appearance in the final image.

A fat suppression sequence, STIR, is included since most LNs contain significant amount of adipose tissue. Metastatic areas and adipose tissue both lack macrophages, leading to no uptake of SPIOs and thus retaining their original MRI intensity after SPIO injection. Therefore, a clear distinction between adipose tissue and metastatic areas is crucial. By using this sequence, fat is suppressed, allowing for a clear distinction[28].

In STIR-, T1-, and T2-Weighted images, multiple scans are acquired and averaged afterwards. While this process increases the total scan time, it significantly reduces noise and therefore increases the image quality. Throughout this thesis, this will be referred to as the "number of averages."

T1 and T2 mapping is a MRI technique used to calculate the T1 or T2 time of tissues and display them voxel-wise on a map[29]. Challenges for SPIO-enhanced MRI LN staging involve quantification of SPIO heterogeneity across a SLN. The current evaluation of T1- and T2-Weighted images is prone to subjectivity[30]. To overcome these challenges and create a general evaluation protocol, MRI maps are included. Rather than a representation of signal intensity, MRI maps depict variations in T1 and T2 values. To generate these maps, a series of MRI images are acquired using sequences with varying echo times (for T2 mapping) or inversion times (for T1 mapping)[29, 31]. The data from these sequences are then fitted to mathematical models that calculate the T1 and T2 relaxation times for each voxel, producing detailed maps. T1 and T2 relaxation times have the potential to serve as independent, tissue specific values and could therefore contribute to a quantitative assessment of the LN.

Table 1 provides an summary of these currently used sequences, along with their duration and number of averages used.

Table 1: Current ex vivo MRI protocol with duration and averages. Resulting in a total scan duration of 340 minutes.

Sequence	Duration(min)	Number of averages
T1-Weighted	53	8
T2-Weighted	160	8
STIR	72	3
T1-Map	29	N/A
T2-Map	26	N/A

### 3 Method

#### 3.1 In vivo evaluation of the DiffMag handheld probe

In vivo measurements of the DiffMag handheld probe were conducted at the UMC Maastricht. Pigs used for the laparoscopic general surgical skills course were surgically prepped and anaesthetised for the purpose of the course. They were humanely euthanized prior to dissection via overdose.

Twenty-five minutes before overdose two magnetic tracers (Magtrace, Ferrnova; 28 mg iron/mL and Ferrotrace; 55 mg iron/ml, Ferrnova) were injected subcutaneously into the both the hind legs. A total volume of 1 mL was injected at four spots in both hind legs subcutaneously. The needle was inserted at an angle  $\approx 15^\circ - 20^\circ$  to the limb surface, needle penetration was  $\approx 5$  mm, and the bevel of the needle was pointing outwards. In the left leg, 1 mL of Magtrace was injected, while in the right leg, 1 mL of Ferrotrace was used. This procedure was performed on two pigs. These injection points were located 15 cm from the tip of the hoof and spaced approximately 1 cm from the center of each quadrant, as shown in Figure 3.1. About 0.25 mL was injected at each site. Following the injections, leg pumps were performed for 30 seconds, and a waiting period of 25 minutes was observed before starting the SLNB to promote lymphatic uptake.

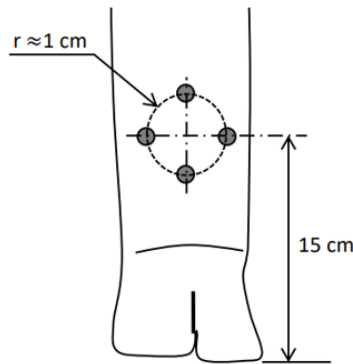


Figure 3.1: Injection sites in the hind leg

The DiffMag probe was utilized to detect in vivo signals from draining inguinal LNs in the groin area. Initially, the groin was scanned transcutaneously using DiffMag (Figure 3.2B), and areas with high signal intensity were identified as magnetic 'hot spots.' These locations were marked with blue pencil crosses (Figure 3.2A). Following this, the skin and underlying structures were carefully removed at these marked spots. If the probe continued to register a high signal, the LN was excised (Figure 3.3). After removal, the LNs were transported to the University of Twente for use in optimizing the ex vivo MRI LN protocol.

During this process, both metal and plastic instruments were used to evaluate the DiffMag's responses to different materials. A metal spreader was used to open the wound and metal tweezers were employed alongside the probe to grasp the tissue and locate the LN.

To assess the representatives of the pig LNs compared to human LNs, magnetic measurements using SPaQ were conducted at frequencies of 2500, 5000, and 7500 Hz. A look-up table (LUT), generated by developers of the SPaQ system[32], was used to calculate the iron content in the pig LN. This iron content was then compared to the iron levels in LNs from the LowMag trial, which involved human SPIO-enhanced LNs.

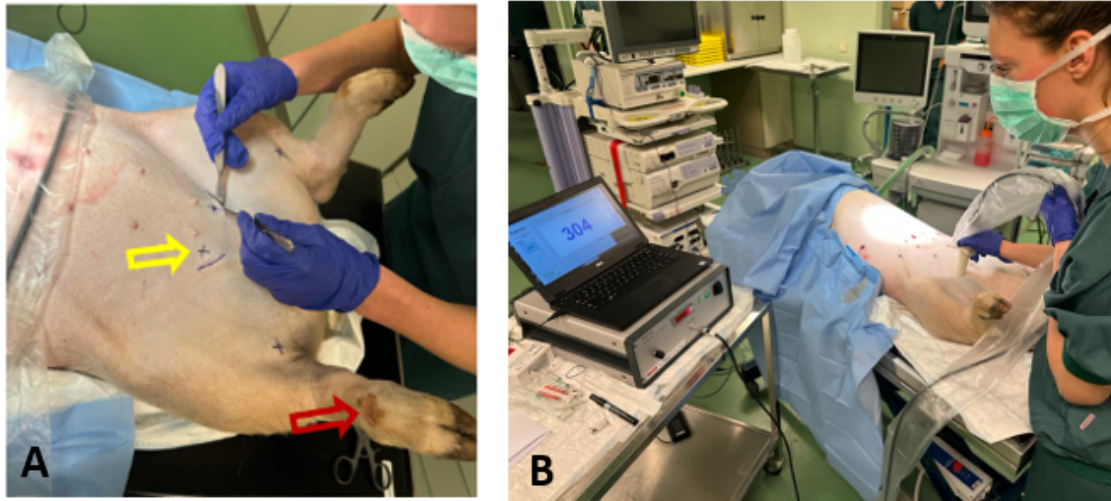


Figure 3.2: In vivo porcine SLNB. A) Injection site indicated with the red arrow and inguinal 'hot spot' indicated with yellow arrow. B) Detection of SPIO-enhanced LNs with the DiffMag probe



Figure 3.3: Porcine LNs during and after removal

### 3.2 Optimization of the ex vivo LN MRI protocol with Compressed Sensing

Previous work implemented CS on the 0.5T tabletop MRI (Pure Devices, Germany) which is used to scan LNs ex vivo (Figure 3.5A)[19]. This implementation was based on the CS toolbox developed by Lustig et al., which was made publicly available[20]. This implementation included a FSE T1-weighted CS sequence with 50% sampling. This CS sequence was tested on a phantom and standardized parameters were used for reconstruction.

The concept of using a dynamic density 2D Poisson disc sampling pattern instead of a classic Cartesian pattern was also implemented. In CS, the k-space design plays a crucial role in the final image reconstruction. In k-space the low spatial frequencies are represented at the center of k-space and high spatial frequencies are located towards the edges[33]. The Poisson disc approach ensures that the central area of the k-space is densely sampled while the peripheral regions receive fewer samples. It also guarantees that the sampled points are randomly distributed, while also ensuring a minimum distance between them, which encourages sparsity. The extreme outer regions of the k-space are not sampled, as these areas typically contain minimal information in a fully sampled image[19]. Figure 3.4 shows the impact of this Poisson disc pattern compared to a Cartesian pattern. Note that this approach is not feasible for 2D imaging, but it is well-suited for 3D CS applications.

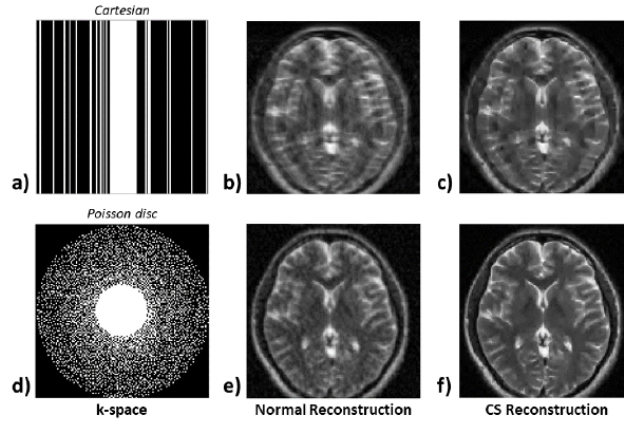


Figure 3.4: CS sampling patterns. Cartesian pattern k-space design (a) with reconstruction (b-c). The Poisson disc design (d) ensures that the central area of the k-space is densely sampled while the peripheral regions receive fewer samples, resulting in a higher image quality (f)[19].

This previous work implemented CS in T1-weighted and designed a Poisson Disc k-space design. However, it did not incorporate CS into T2-weighted images and MRI maps, nor did it explore different Poisson disc sampling patterns or the effect of the regularization parameter on the reconstruction outcome.

### 3.2.1 Compressed Sensing in T1- and T2-Weighted Fast Spin Echo MRI

To integrate CS in T2-weighted images and to evaluate effects of alternative k-space patterns, the obtained pig LNs from the in vivo experiments were used. Excessive fat from the LNs were removed and they were placed in a tube filled with formaldehyde. The bottom of the tube was filled with plastic to ensure the LN was within the field of view (FOV) of the table top MRI(Figure 3.5B).

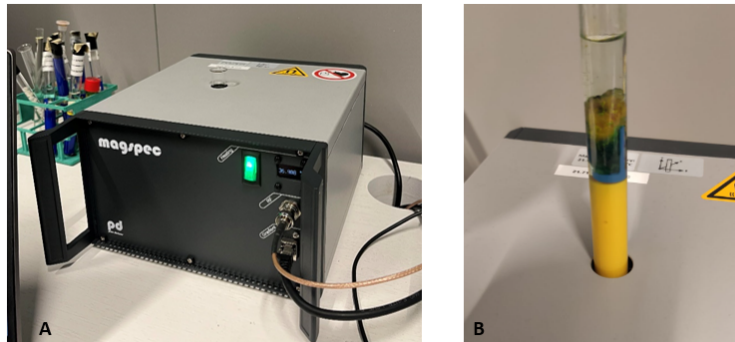


Figure 3.5: Overview of the table top MRI A) The table top MRI system B) Colored LN in formaldehyde before scanning

Initially, the pig LNs were scanned with a fully sampled pattern utilizing a 3D FSE sequence, with parameters set as shown in Table 2.

Table 2: MRI Parameters FSE sequences

Parameter	T1-Weighted	T2-Weighted
Echo Time(ms)	4.5	4
Repetition Time(ms)	450	4000
Isotropic resolution(mm)	0.25	0.25
Bandwidth(Hz/voxel)	500	500
Turbo factor	4	4

Immediately following this fully sampled scan, the scan was repeated with the same parameters but now using sampling rates of 50% and 25%. The Poisson disc sampling pattern was used for these scans and they were reconstructed afterwards with the Lustig reconstruction[20]. During reconstruction, the standardized values of 15 iterations and 0.005 for the regularization parameter were used. The reduction in k-space points during this process can sometimes result in artifacts known as Gibbs ringing[34]. Gibbs ringing is an artifact where oscillations or ripples appear at the edges of structures, caused by abrupt changes in intensity within the image. This issue is avoided by smoothing the sharp edges of the k-space with a hamming window (Figure 3.6).



Figure 3.6: k-space before and after smoothing with a hamming window

To enhance the performance of the Poisson disc pattern, variations in the diameter of its central part were explored. Initially, the central disc had 47% of the sampled area, which was then increased to 57% and 67% (Figure 3.7). Comparison of the reconstructed images was performed using the evaluation matrix described in section 3.2.3.



Figure 3.7: Poisson disc pattern with varied Centre parts

### 3.2.2 Regularization parameter

To explore the effects of varying regularization parameter values on the reconstructed image, a fixed number of averages of 4 and 2 were maintained, and two different sampling percentages—50% and 25%—were examined. A range of regularization parameter values from 0.0005 to 2 was tested. The results were assessed using the evaluation matrix described in Section 3.2.3.

### 3.2.3 Image quality assessment

The CS images were compared to the fully sampled 16 average image. The LN was segmented to focus solely on the relevant areas. The image quality of the reconstructed images was evaluated using Peak Signal-to-Noise Ratio (PSNR), Mean Squared Error (MSE) and Structural Similarity Index Measure (SSIM) metrics.

1. PSNR measures the quality of an image by comparing it to a reference image. It calculates the ratio of the maximum possible power of a signal to the power of corrupting noise that affects the accuracy of its representation. Higher PSNR values indicate lower levels of noise and better image quality.
2. MSE is a commonly used metric to quantify the difference between two images. It computes the average squared differences between the pixels of the original and the distorted images. Lower MSE values suggest less distortion and higher image quality.
3. SSIM is a metric used to measure the similarity between two images. It takes into account the luminance, contrast, and structure of the images. A higher SSIM value indicates a greater similarity between the images, implying better quality.

### 3.2.4 Compressed Sensing in MRI maps

CS was integrated into T1 and T2 MRI maps using the Poisson disc pattern as k-space design. This undersampled k-space was generated prior to scanning and used consistently across all scans with varying TEs or TRs. To reconstruct the undersampled maps, the individual scans per acquisition time were temporally separated and reconstructed individually. The regularization parameter was set to 0.005. After reconstruction, the scans were reintegrated into a single reconstructed scan, accommodating with the varying acquisition times.

From this reconstructed scan, a MRI map was generated using a fitting technique. In this approach, the transverse relaxation time was estimated by fitting the acquired signal intensities (SI) against the TEs or TRs, employing Equation 2 as the fitting model. To ensure an accurate fit, initial values were selected within the range of expected values for each voxel. Consequently, parameter a was initial set to the maximum signal intensity value. The starting value for T1 and T2 were determined at the point where the signal intensity equaled 0.63 for T1 and 0.37 for T2. Parameter c, representing the potential offset, was set to the mean of the signal intensity.

$$SI = a * e^{\frac{-TE}{T2}} + c \quad (2)$$

## 4 Results

### 4.1 In vivo evaluation of the DiffMag handheld probe

Two hotspots were transcutaneously identified with the DiffMag handheld probe when no surgical instruments were near the probe. During this transcutaneous measurements, the SLNs produced approximately 100 DiffMag counts (Figure 4.1b). The DiffMag needed to be balanced once throughout the procedures. No drift was observed in the readings of the device over time. A filled-in questionnaire about the usability of the DiffMag can be found in Appendix C.

The device detected a minimum of 400 counts when tweezers were placed close to the tip of the DiffMag probe when kept stable (Figure 4.1e). These readings increased up to 6210 counts as the probe moved closer to the tweezers (Figure 4.1c). The DiffMag showed red counts when the metal surgical instruments were moved around the DiffMag probe.

Based on the ex vivo measurement of the LNs, iron contents of 20.6, 115.4, and 20.3  $\mu\text{g}$  were calculated.

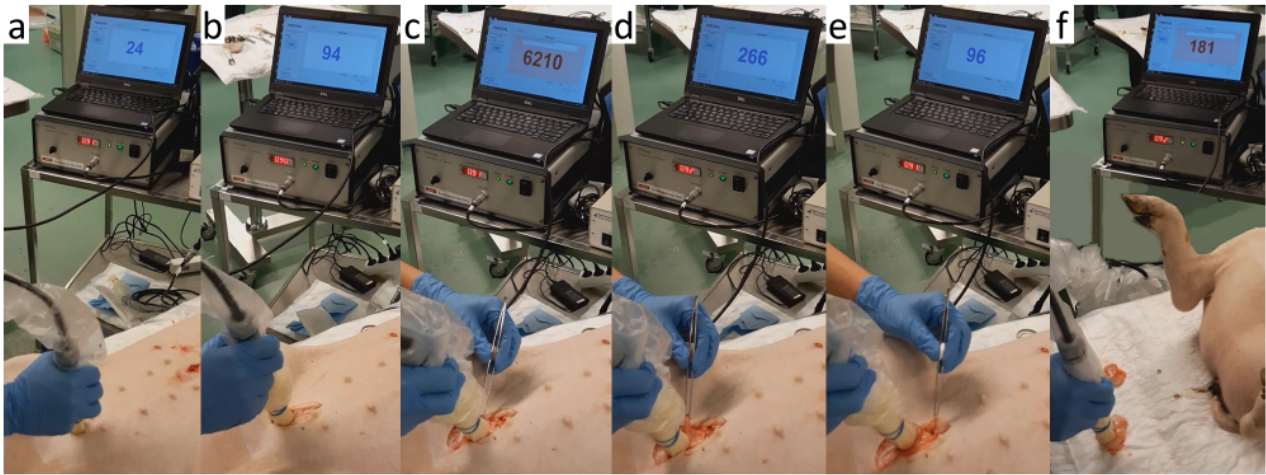


Figure 4.1: DiffMag counts measured at various points during the SLNB. a) Transcutaneously measured. b) Measured in the incision. c) DiffMag signal artifact in presence of a ferromagnetic pair of tweezers. d) Misleading impression of LN presence due to the pair of tweezers. e) Measurement directly on LN. f) Ex vivo measurement of LN on a metal table.

### 4.2 Optimization of the ex vivo LN MRI protocol with Compressed Sensing

#### 4.2.1 Compressed Sensing in T1- and T2-Weighted Fast Spin Echo MRI

Figure 4.2 present an overview of T2-weighted FSE scans of a pig LN using sampling percentages of 100%, 50%, and 25% with 2, 4, 8 and 16 averages. SSIM scores of the images are given in Figure 4.3.

The PSNR for the 100% sampled images is 22.3 for 2 averages, 27.3 for 4 averages, and increases to 32.4 for 8 averages. In comparison, the PSNR for the 50% sampled images is 22.318 for 2 averages, 24.904 for 4 averages, and rises to 25.80 for 8 averages. While the difference in PSNR is minimal at lower averages, there is a substantial disparity at 8 averages.

Figure 4.4 shows T1-weighted FSE scans of another pig LN with 100% and 50% sampling, which gave similar results. SSIM score for 50% 2 average scan was 72.49% and increased to 73.87% for the 4 average scan and 79.65% for the 8 average scan.

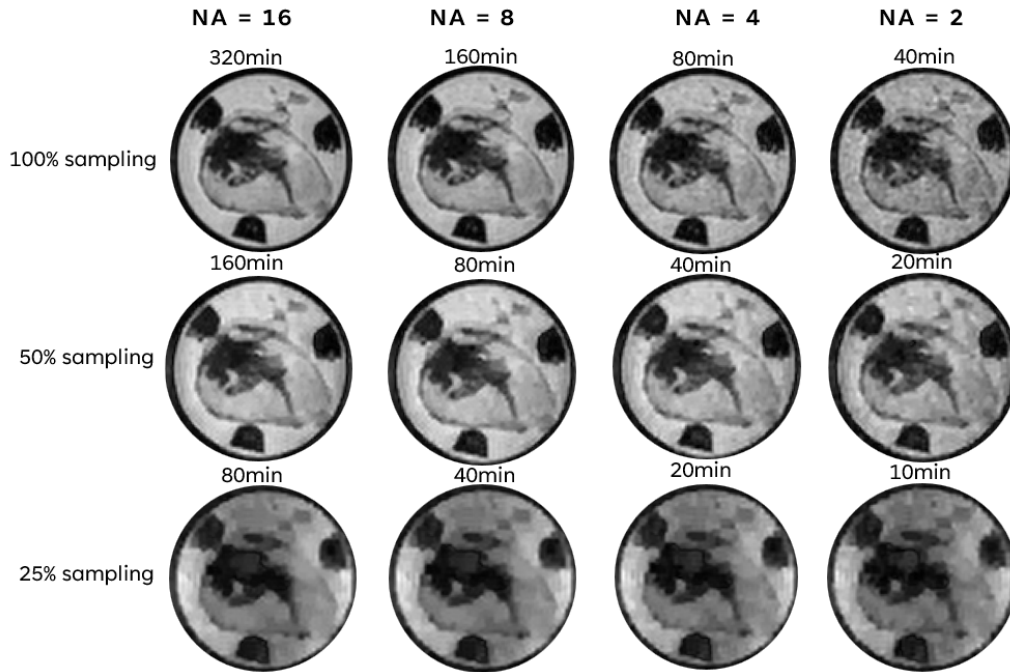


Figure 4.2: Pig LNs T2 weighted MRI FSE scans with different sampling rates and averages. Images become sparser as the sampling percentage decreases. Scans at 25% sampling are sparse and display less detail compared to those at 100% and 50%, even when utilizing 16 averages. However, images at 50% sampling remaining recognizable and details still observable and closely resemble the scans with 100% sampling rate.

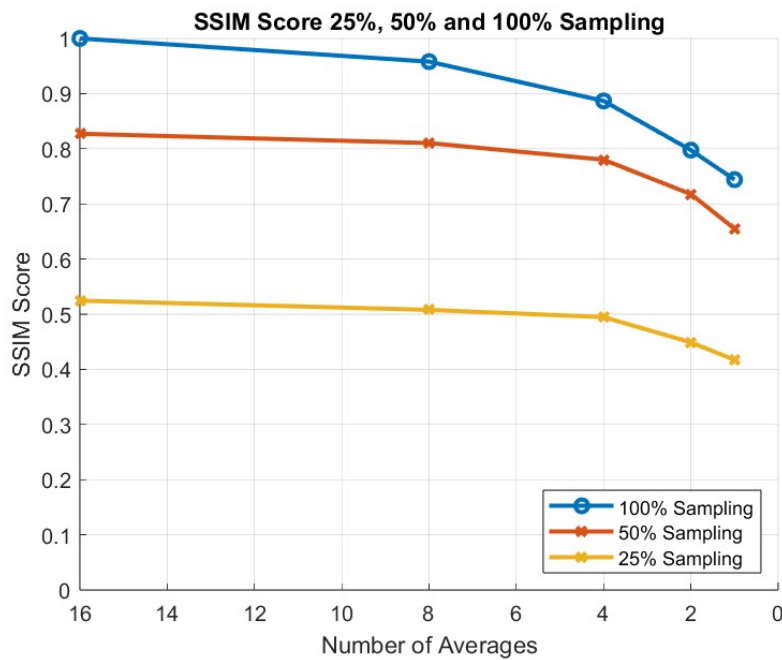


Figure 4.3: SSIM score of 25%, 50% and 100% sampling. The SSIM score of the 25% sampling starts at 52% and decreases to 0.41%, the 50% sampling starts at 82% for 16 averages and decreases to 65% for 1 average. The 100% sampled image starts at 1, as this is the reference image, and decreases to a SSIM score of 74% for 1 average. For the lower averages, the SSIM score of the 50% sampled image is approximately 10% lower than that of the 100% sampled image with the same number of averages.

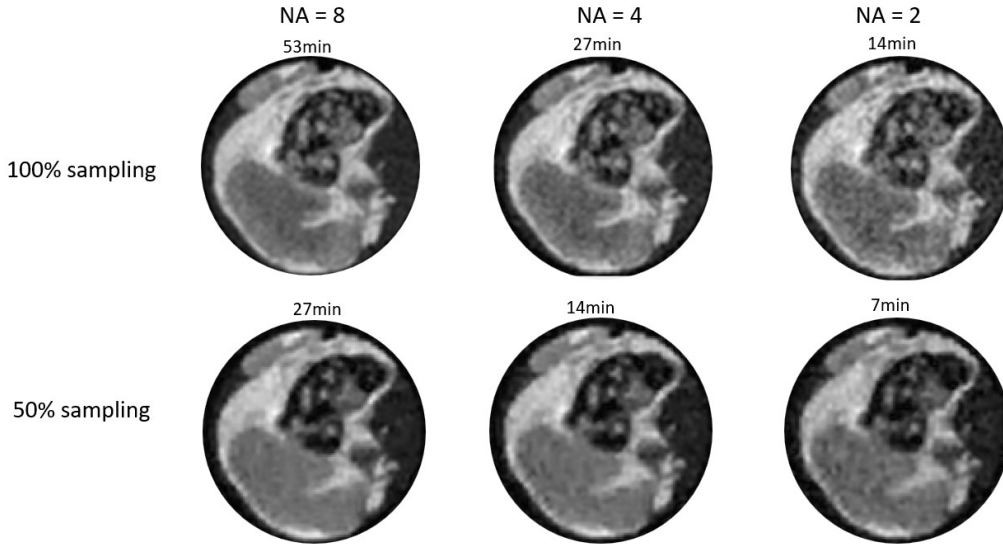


Figure 4.4: T1-weighted MRI scans of a pig LN with 50% and 100% sampling

Figure 4.5 displays T2 FSE scans of a pig LN obtained using compressed sensing with a Poisson disc pattern, where the central part of the disc varies. Table 3 provides quantitative metrics, including SSIM, PSNR, and MSE, comparing these scans to a fully sampled 16 average scan. The image featuring a 57% central area (Figure 4.5B) demonstrates slightly better performance, achieving a SSIM score of 78.0% compared to 76.3% and 75.4% for the other scans. Also the PSNR and MSE performed slightly better, with 24.9 compared to 24.1 and 24.6 and 0.0032 compared to 0.0038 and 0.0035 respectively.

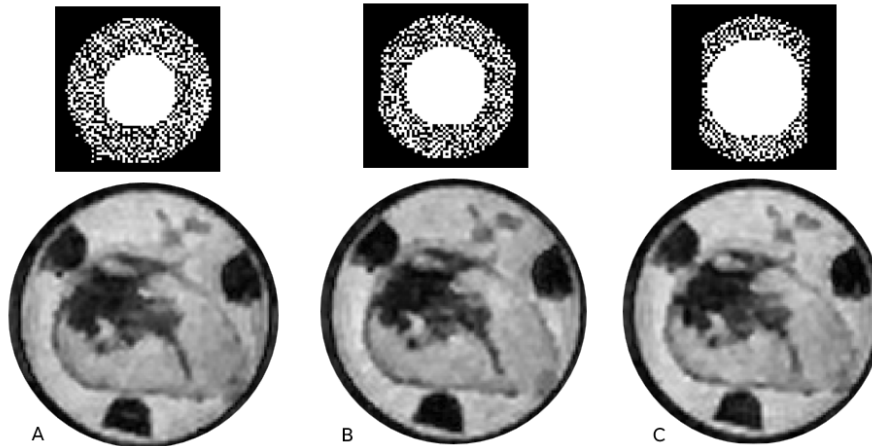


Figure 4.5: T2 FSE scan of a pig LN with varying centres of poisson disc

Table 3: T2 FSE scans with varying centre disc pattern compared to fully sampled image with 16 averages.

NA	sampling(%)	Disc Centre	SSIM(%)	PSNR	MSE
4	50	0.47	76.322	24.175	0.0037875
4	50	0.57	78.011	24.9034	0.0032027
4	50	0.67	75.387	24.5611	0.0034653

Figure 4.6 provides an overview of four different scans with varying regularization parameters and averages. Table 4 displays the comparison between these scans and the fully sampled 16 average scan. Table 4 summarizes the results of these scans with varying regularization parameters and numbers of averages at a consistent sampling rate of 50%. For 2 averages, as the regularisation parameter increases from 0.005 to 0.2, SSIM values range from 71.77 to 72.11, while PSNR slightly fluctuates between 22.31 and 23.62. The corresponding MSE values show a decrease from 0.0058 to 0.0043. When the number of averages is increased to 4, the SSIM values

improve across all regularisation parameters, reaching a maximum of 78.01 at regularisation parameter is 0.005. Similarly, the PSNR increases to a maximum of 24.90 at the same regularisation parameter, with MSE values decreasing to as low as 0.0032.

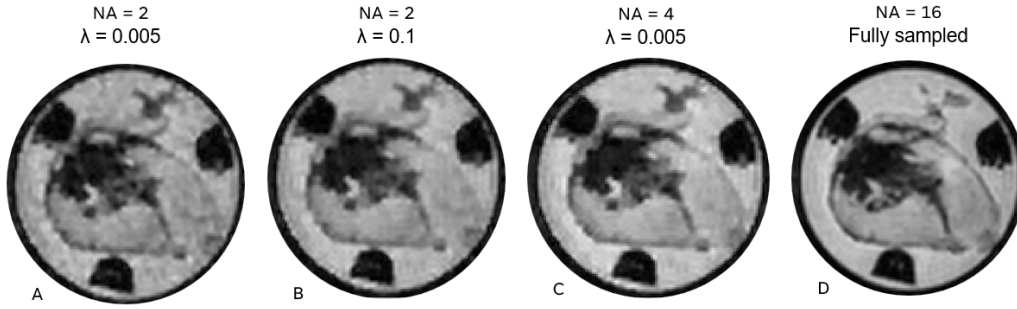


Figure 4.6: T2 FSE scan of LN A) 2 Averages and with  $\lambda$  set to the original value (0.005) B) 2 Averages with  $\lambda$  increased to 0.1 C) 4 Averages with  $\lambda$  set to original value (0.005) as used in the LowMag trial D) Fully sampled image with 16 averages

Table 4: T2 FSE scans with varying regularisation parameter ( $\lambda$ ) and NA

NA	sampling(%)	$\lambda$	SSIM(%)	PSNR	MSE
2	50	0.005	71.77	22.31	0.0058
		0.1	72.48	23.62	0.0043
		0.2	72.11	22.91	0.0053
4	50	0.005	78.01	24.90	0.0032
		0.1	76.534	23.75	0.0041
		0.2	74.839	23.10	0.0049

#### 4.2.2 Compressed Sensing in MRI maps

Figure 4.8 shows the fully sampled T2-map (Figure 4.8A) and the T2-map obtained with CS (Figure 4.8B) of a pig LN. It reveals that the map obtained with CS results in higher T2 values. While the SPIO area retains values around 0, consistent with the fully sampled map, the LN tissue gives higher values ranging from 0.2 to 0.25.

The T1-map generated with CS shows results comparable to the T2-map. Figure 4.7 presents both the fully sampled T1-map (Figure 4.7A) and the T1-map obtained using CS (Figure 4.7B), with the CS map displaying higher T1-values than the fully sampled map.

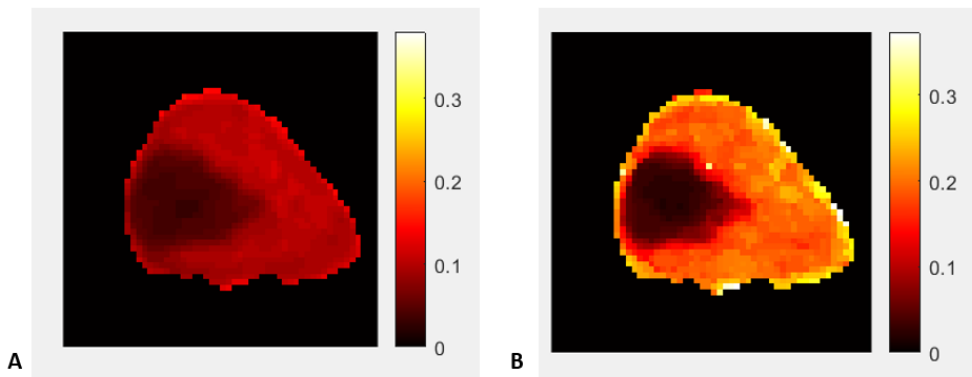


Figure 4.7: T2 maps with T2 values in seconds A) T2-map fully sampled B) T2-map with compressed sensing. The fully sampled map shows lower T2 values compared to the map acquired with CS

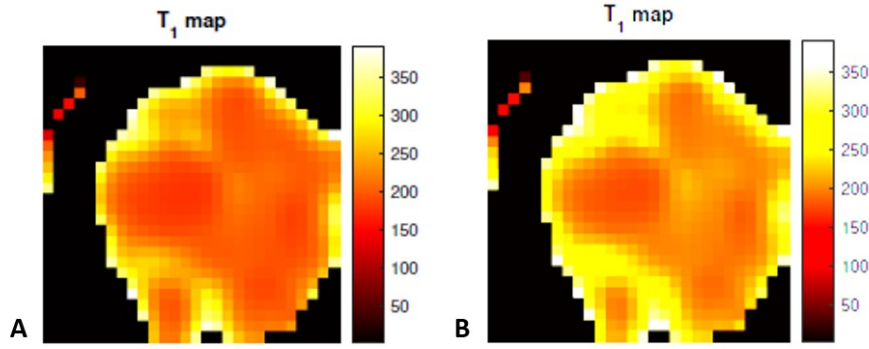


Figure 4.8: T1 maps with T1 values in seconds A) T1-map fully sampled B) T1-map with CS. The fully sampled map shows lower T1 values compared to the map acquired with CS

The intensity values of two pixels in the T2 map in the SPIO and LN areas, with and without CS, were analyzed and are presented in Figure 4.9. The figure illustrates that the T2 values obtained without CS produce smoother curves compared to those with CS in both the SPIO area (left) and the LN area (right). The data points in the curves without CS show less fluctuation and more gradual transitions, particularly at the lower echo times.

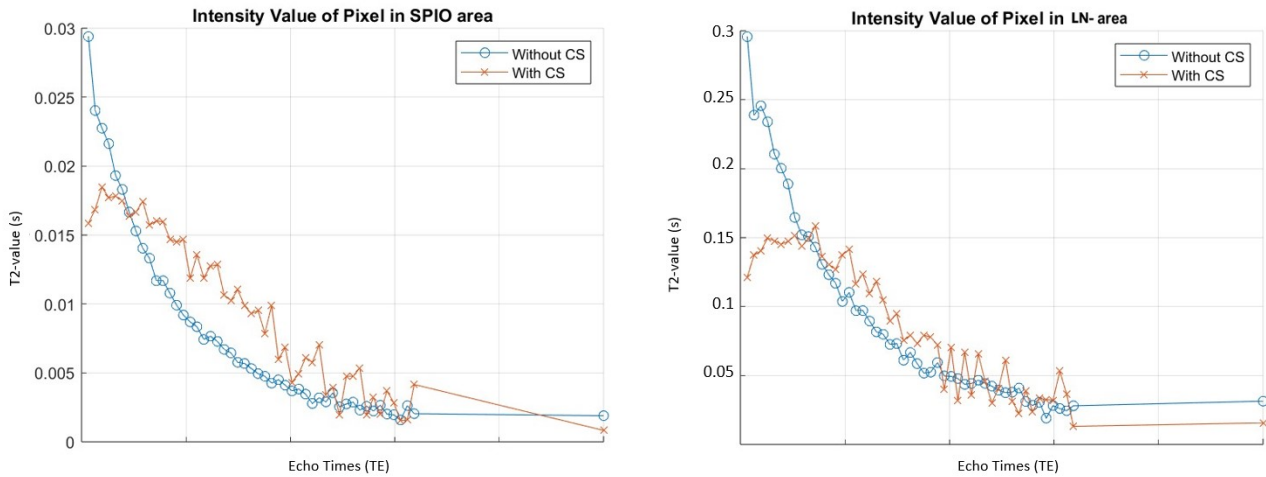


Figure 4.9: Intensity values of one pixel within the SPIO area (A) and one within the LN area (B) plotted over different TE's. For the map without CS, the intensity values start at approximately 0.03 and gradually decrease, showing a smooth decline with some fluctuations, stabilizing around 0.005. In the map with CS the intensity values start around 0.15, and exhibit more variability compared to the measurements without CS.

The intensity values of T2 maps for the SPIO and LN area with and without CS were analyzed and are presented in a boxplot in Figure 4.10. The boxplot compares the intensity values across four different areas: CS LN area, CS SPIO area, Normal SPIO area, and Normal LN area. The CS LN area showed a median intensity value around 0.2, with the interquartile range (IQR) spanning from approximately 0.15 to 0.22. A number of outliers were observed above and below this range, indicating some variability in the intensity values within this region. The SPIO area in the map without CS displayed a median intensity value around 0.075, with an IQR from approximately 0.05 to 0.1. In the CS SPIO area, the median intensity value was lower, around 0.1. The IQR for this region ranged from approximately 0.05 to 0.12. The LN area had an intensity value of around 0.05, with an IQR from approximately 0.025 to 0.075.

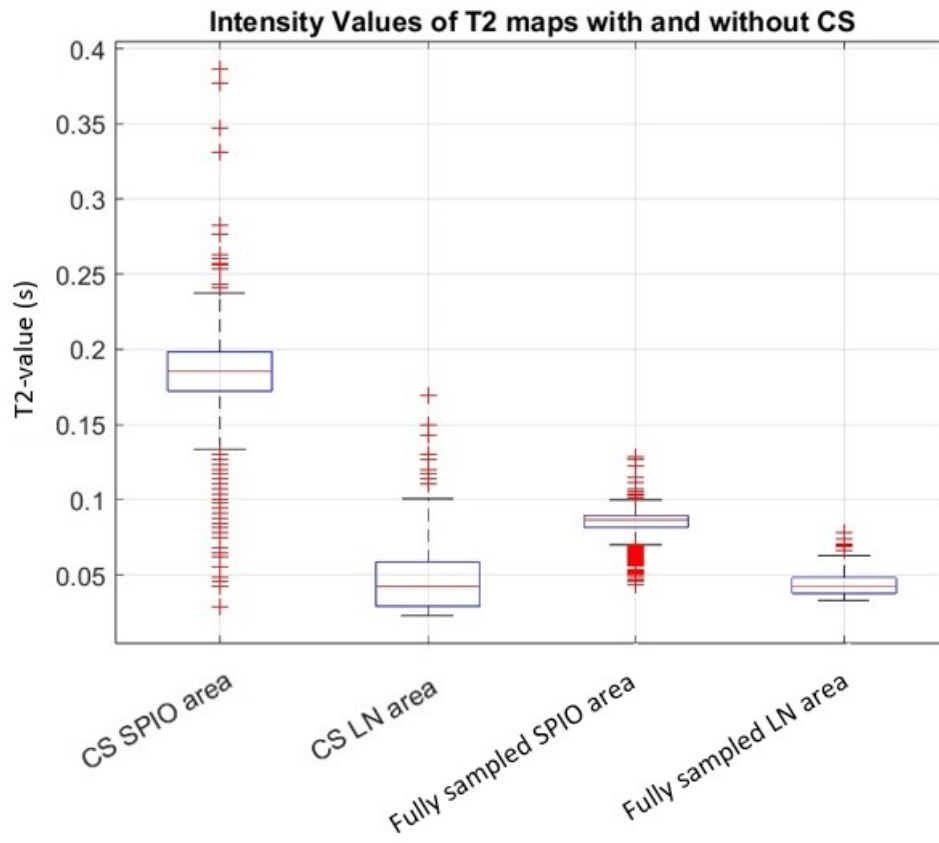


Figure 4.10: Boxplot of T2-values of T2-maps with and without CS. CS map show higher T2-values than the fully sampled map.

## 5 Discussion

The thesis aimed to optimize the implementation the MelaDiff trial protocol. This involved performing an in vivo evaluation of the DiffMag handheld probe and integrating CS into the ex vivo LN MRI protocol.

Compared to the SentiMag, the DiffMag probe demonstrated advantages in LN detection accuracy and overall user-friendliness during in vivo use. While both systems are simple, making them accessible for first-time users, the DiffMag probe stands out for its performance and ease of operation. The SentiMag requires recalibration approximately every 30 seconds and is prone to signal drift. The DiffMag showed no signs of drifting and needed to be balanced only once at the beginning of the procedures, which typically lasted about 45 minutes. Once the DiffMag probe is set down, its signal resets to zero, and when picked up again, it immediately resumes accurate functioning. This responsiveness allows for quicker and more reliable identification of SPIO-enhanced SLNs. In clinical practice, especially in challenging SLNB procedures where LN identification can be difficult, the DiffMag’s consistency and stability can reduce procedure time and complexity. The absence of recalibration and signal drift not only streamlines the process but also enhances the overall efficiency and user experience, making the DiffMag a more reliable and user-friendly device compared to the SentiMag.

During the procedures, the DiffMag measurements were influenced by nearby metallic surgical instruments. Given the claims that it was unaffected by other diamagnetic materials[13], the DiffMag did not perform as well as expected. Similar to the SentiMag, the DiffMag device exhibited significantly higher counts when metal equipment came within approximately 3 cm of the probe. Even when both the probe and the surgical equipment were kept stable, the DiffMag device continued to display higher counts compared to when the equipment was farther away. This suggests that the principle, as shown in Figure 2.2, is not working as intended. Further research has been initiated to identify why the DiffMag is malfunctioning in term of influence from metal and proposed possible solutions[35]. In this work, two primary sources were identified for the signal artefacts: 1) The magnitude of DiffMag counts depend not only on the amount of SPIONs and the distance between them and the probe, but also on the speed at which the probe moves towards or away from the sample. 2) The changing magnetic flux generates a magnetic field that opposes the applied magnetic field. This opposing field reduces the overall magnetic effect, leading to a decrease in the measured voltage, even though the paramagnet’s positive susceptibility would normally increase it. A proposed solution for these issues involves phase-shift-dependent signal detection. The phase shift of SPIONs can be easily identified even with the presence of surgical metal instruments and should theoretically solve the problem. Further research must reveal whether these updates are sufficient. Until this metallic interference issue is fully addressed the DiffMag probe may be considered to impractical. With the current DiffMag device, surgeons are still forced to switch to plastic instruments during the procedure and afterwards relocate the SLNs. This undermines the probe’s effectiveness, makes it impractical for use in the operating room and increases the duration of the procedure.

An appropriate working magnetometer becomes even more important with the newly introduced radiation-free methods for SLN detection, such as IndoCyanine Green (ICG). ICG, a fluorescent dye, can effectively highlight lymphatic vessels and nodes during surgery, while allowing for the continued use of metallic surgical equipment[36, 37]. However, while ICG is efficient at identifying SLNs, it does not facilitate preoperative LN mapping or staging. For this reason, SPIOs provide a more comprehensive approach as it also allows for preoperative staging and mapping. When combined with a properly functioning magnetometer, SPIOs offer an advantage over ICG due to their multiple capability. However, if the magnetic probe does not function optimally, a combined approach using both SPIOs and ICG might become the new standard of care[38].

One of the limitations of the in vivo comparison of DiffMag and SentiMag is that the SentiMag could not be used alongside the DiffMag during the porcine measurements, due to hygiene concerns. For this reason the SentiMag’s performance was based on clinical experience from the LowMag trial, which involves SLNBs on breast cancer patients. However, the porcine procedures were not fully representative for a typical clinical scenario as where the SentiMag was evaluated on. The iron content in the pig LNs was 120.6, 115.4, and 20.3  $\mu\text{g}$ . In comparison, the LowMag trial reported iron levels ranging from 0.1 to 109  $\mu\text{g}$  in human LNs[14], making the third LN’s iron content within the clinically representative range for human LNs. However, the first two LNs, with higher iron levels, were likely easier to detect. Additionally, the pig LNs might be located more superficial than typically seen in human axillas. This could have influenced the effectiveness of SLN detection using the DiffMag in the porcine model. Nevertheless, the use of surgical equipment and the recalibration of the DiffMag during these tests were fairly representative, as the same equipment and procedures were employed as in clinical practice, including the handling of the probe. For this reason, these porcine tests provided initial insights into the DiffMag probe’s performance relative to the SentiMag and offered valuable information on its interaction with surgical equipment. However, the upcoming MelaDiff trial will be crucial in determining whether the DiffMag probe maintains its stability and effectiveness in more complex SLNB procedures and

whether the issue with metallic interference can be solved.

Besides the evaluation of the Diffmag handheld probe, this thesis also focused on integrating CS into the ex vivo LN MRI protocol to make the imaging process less time-consuming. In the LowMag trial all scans were fully sampled, and for both T1- and T2-weighted scans, 8 averages were taken. This resulted in a total scan time of 340 minutes ( $\approx$  6 hours) per LN. This lengthy image process makes the clinical applicability of SPIO-enhanced MRI staging unfeasible and hinders research efficiency. This thesis successfully implemented CS in T1- and T2-weighted images, but its integration into MRI maps has revealed some irregularities that require further investigation.

Analysing T2-weighted FSE scans with and without CS, the SSIM scores, as expected, increased with higher sampling percentages and a greater number of averages. Nevertheless, the image with 50% sampling with 16 and 8 averages keeps recognizable details and closely resembled the fully sampled images. Even with averages set to 4, the LN remains clearly visible, which is supported by the little decrease of the SSIM score. On the contrary, the 25% sampled images are significantly sparser and display less detail, even with an increased number of averages. This is also indicated by the much lower SSIM score. For this reason, the 25% sampling is deemed insufficient for maintaining acceptable image quality.

When further analysing the 50% sampled image, it was found that the optimal regularisation parameter for the 4 averages scan was a value of 0.005. This gave the highest SSIM score (Figure 4.6 and Table 4). For the 2 averages scan, the highest SSIM score was found by setting the regularisation parameter to 0.1. A visual inspection confirmed this, as the image shows less noise. Analysing the varying central area part of the poisson disc reveals that the image with a 57% central area has a slightly better SSIM score. This is possibly due to the better preservation of crucial image information in the higher k-space frequencies while maintaining enough information in the lower frequencies. For this reason, T2-weighted image with a sampling rate of 50%, a central sampling part of 57% and 2 averages, reconstructed with regularisation parameter of 0.1, is deemed sufficient. This reduces the scan time with 140 minutes (from 160 minutes without CS to 20 minutes with CS).

T1-weighted images show similar results in the effects of sampling percentages and averages on the image quality (Figure 4.4). The 25% sampled images lack too much detail and images with 50% sampling rate and 4 averages still produce sufficient results. Efforts were made to achieve better results with the 2 averages scan by increasing the reconstruction parameter to 0.1. The SSIM score did improve, but visual inspection indicated that it was insufficient to visualise clear borders. The boundaries of the SPIOs were not clearly visible and did not closely resemble those in the fully sampled image. Additionally, increasing the number of averages from 2 to 4 adds only 7 minutes to the total scan time. So for these two reasons, the 4 averages scan with a reconstruction parameter of 0.005 is preferred. This reduces the scan time with 39 minutes (from 53 minutes without CS to 14 minutes with CS). Table 5 gives an overview of the updated parameters of the ex vivo MRI protocol, as can be used in the MelaDiff trial, derived from the above considerations.

Table 5: Updated ex vivo MRI protocol parameters

Parameter \ Weighting	T1	T2
Number of averages	4	2
Sampling rate (%)	50	50
Sampling pattern	Poisson Disc (57% center part)	Poisson Disc (57% center part)
Regularisation parameter $\lambda$	0.005	0.1
Duration (min)	14	20
Time saving (min)	39	140

For CS in MRI mapping, the boxplots suggest that the contrast between the SPIO area and the LN area is more pronounced in the CS map than in the fully sampled map. The T2-values of the fully sampled in the SPIO area of the map are lower than those in the 50% sampled map, while the T2-values in the LN area maintain approximately the same value. This enhancement could potentially improve visibility of SPIOs in MRI images. However, these results indicate that scanning MRI maps with a lower sampling rate influences the outcome of the map. Although the sampling pattern was kept constant over different scans with varying TEs, it suggests that the sampling rate introduces a difference compared to the 100% sampling pattern. This is also seen in Figure 4.9, which exhibits significant fluctuations in the CS map plot, rather than a smooth curve as in the fully sampled map plot. This may be due to the individual reconstruction of the scans. The scans are splitted before reconstruction, introducing a individual component in terms of intensity values. This could lead

to different intensity values after reconstruction. Nevertheless, increased contrast between SPIOs and LN tissue may potentially improve the evaluation of SPIO distribution. However, it remains uncertain if this accurately represents the true distribution. A recommendation for further analyse would be to acquire slices of the LN and lay them alongside the MRI maps to assess whether the CS MRI map accurately reflects the true distribution.

Although CS is not ready to be implemented into MRI maps, it was successfully implemented in T1- and T2- weighted FSE MRI sequences. Leaving the total scan procedure with T1-, T2-, STIR- weighted and T1- and T2-map scans at 144 minutes ( $\approx 2.5$  hours). Resulting in a total time saving of 179 minutes ( $\approx 3.5$  hours). This reduction in scan time moves SPIO-enhanced staging closer to being clinically applicable. Additionally, it enhances the practicality of research by allowing the integration of other imaging sequences. One of these sequences is DIXON. DIXON is a fat suppression sequences, which enables the distinction between malignant LN tissue and benign adipose tissue. Since SPIOs are also not present in adipose tissue it is very important to identify this tissue. Studies were set up to explore the potential of DIXON sequence[39].

While SPIO-enhanced MRI shows promise as a non-invasive method for accurate LN staging and significant progress has been made, multiple research steps are necessary to fully explore its clinical potential. Firstly, a crucial step involves comparing ex vivo MRI scans of LNs with their corresponding pathological slices. This comparison allows for the accurate identification of metastatic regions on the pathological slice, which can then be correlated with the ex vivo MRI scan. To facilitate this a protocol was designed in the LowMag trial which included staining of pathological slices with iron, macrophages, and tumor cells staining[14]. This enables the precise localisation of specific cells and allows for a cell-based comparison with MRI scans. The LowMag trial made important initial strides, but more data is needed to make an accurate comparison.

Following the exploration of ex vivo MRI scans, the next step is to extend this research to in vivo MRI, as the ultimate goal is to accurately stage LNs non-invasively. To achieve this, pre-contrast MRI scans can be compared with post-contrast MRI scans. These results can then be aligned with pathological slices to identify metastatic areas.

Finally, for such a method to be truly valuable in daily clinical care, both the sensitivity and specificity must meet a high threshold. High specificity is essential because false positives could lead to unnecessary interventions, which can cause severe complications for the patient without any clinical benefit. Equally important is the sensitivity. High sensitivity is crucial because missing metastatic cells in the LNs could lead to undertreatment, depriving the patient of essential therapy and potentially reducing their chances of survival. Another important consideration is the accuracy of the SPIO-enhanced MRI scans. If the scan cannot definitively rule out the presence of metastatic cells, many patients still need to undergo a SLNB. This may result in added stress and confusion for patients. Additionally, if it occurs too often, it complicates clinical practice and increases costs, making it impractical. Figure 5.1 provides an overview of the stages.

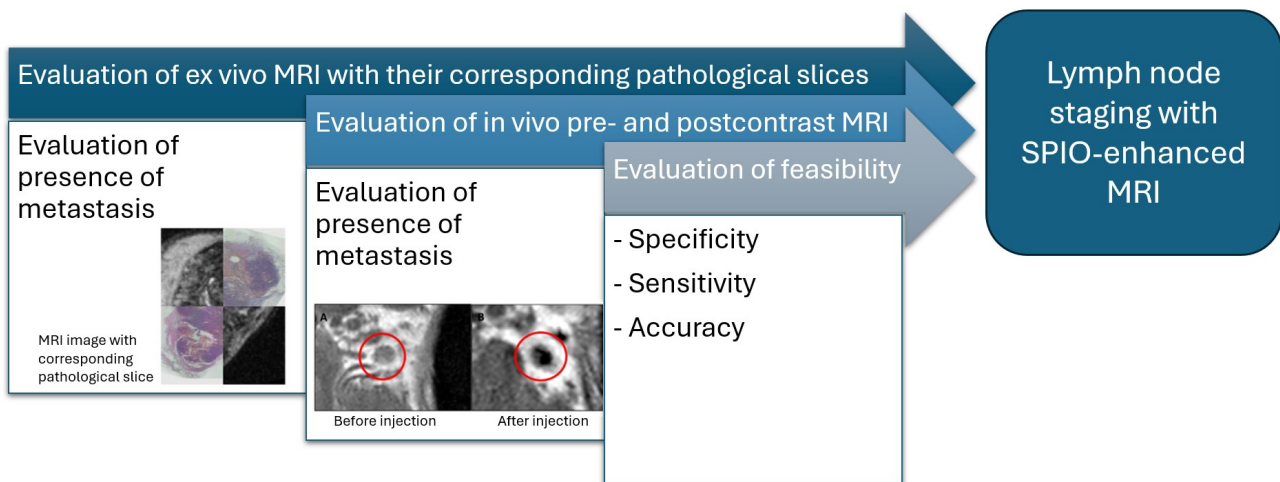


Figure 5.1: Overview of the research stages for investigating LN staging using SPIO-enhanced MRI: Initially, ex vivo MRIs are analyzed to achieve a higher resolution of metastatic and non-metastatic SPIO-enhanced LNs, allowing for a detailed examination of SPIO distribution patterns in these tissues. Next, in vivo MRI scans are assessed to determine the potential for SPIO-enhanced in vivo evaluation and to verify if the patterns observed ex vivo are seen in vivo. Finally, the method’s feasibility is evaluated in terms of sensitivity, specificity, and accuracy, to determine the added value of this approach in daily clinical practice.

Literature is already exploring this in vivo evaluation of LNs with (U)SPIO-enhanced MRI and is showing varying results regarding sensitivity and specificity. Research in breast cancer patients with USPIO-enhanced MRI utilizing the pre- and postcontrast scan gave sensitivity and specificity of 86.4% and 97.5% respectively[26]. The results of USPIO postcontrast images alone were 84.7% sensitivity, 96.8% specificity. Additionally, Motomura et al. have showed that SPIO-enhanced MRI, including a T1-, T2\*-Weighted and fat-suppression sequence, can predict SLN status[40]. The sensitivity, specificity and accuracy were 100%, 96% and 96% respectively. However, the MAGMEN trial included 15 cutaneous melanoma patients from which micrometastatic deposits were identified in four SLNs taken from three patients. SPIO enhanced-MRI correctly predicted two of the metastases using T1-, T2- and T2\* Weighted sequences along with DIXON, indicating a sensitivity of only 50%[10]. The two false negative SPIO-MRI predicted SLNs were both containing metastases measuring <0.1 mm. The interpretation of the SLN status can thereby be challenging due to the size of the metastases. On the contrary, the first two studies also included micrometastase and show, for this reason, promising results for SPIO-enhanced MRI staging in clinical practice. Nevertheless, additional clinical trials must indicate whether SPIO-enhanced MRI staging can consistently achieve these high thresholds for specificity, sensitivity, and accuracy.

## 6 Conclusion

This thesis has taken steps towards optimizing the implementation of the MelaDiff trial protocol by evaluating the DiffMag handheld probe in vivo and optimizing CS in the ex vivo LN MRI protocol. The evaluation of DiffMag shows that the DiffMag probe offers advantages over the SentiMag in terms of user-friendliness and consistency during in vivo use. However, challenges related to interference from surgical equipment persist. The MelaDiff trial must indicate if the DiffMags' advantages over the SentiMag holds up during real surgery, and whether software updates can effectively address the interference issues.

The integration of CS into T1- and T2-weighted MRI sequences reduces the ex vivo scan time by 179 min while maintaining sufficient image quality. This reduction in scan time makes SPIO-enhanced MRI staging more clinically feasible by decreasing the time of the imaging process. Additionally, in research, it allows for the integration of other sequences in the same scan duration. However, further investigation is required to address the limitations identified in integrating CS in MRI mapping.

Looking ahead, the upcoming MelaDiff trial will be the next step in determining whether the DiffMag handheld probe can offer clinical value and whether SPIO-enhanced MRI can establish itself as a reliable, non-invasive alternative for LN staging. If successful, this method could improve patient care by reducing the need for invasive SLNBs, provided it demonstrates high sensitivity, specificity, and clinical practicality. While challenges persist, the foundation laid by this research represents a step forward in melanoma staging. These steps bring us closer to a non-radioactive LN staging procedure that provides prognostic information and guides appropriate treatment strategies, while sparing most patients the potential complications associated with SLNBs.

## References

- [1] “IKNL.huidkanker-in-NL\_rapport\_NKR”. In: ().
- [2] Federatie Medisch Specialisten. *Richtlijndatabase Melanoom*.
- [3] József Tímár and Andrea Ladányi. *Molecular Pathology of Skin Melanoma: Epidemiology, Differential Diagnostics, Prognosis and Therapy Prediction*. May 2022. DOI: [10.3390/ijms23105384](https://doi.org/10.3390/ijms23105384).
- [4] Gianni Gerlini et al. *Melanoma metastases occurring 40 years after primary melanoma*. Oct. 2018. DOI: [10.1080/0284186X.2018.1481295](https://doi.org/10.1080/0284186X.2018.1481295).
- [5] Islam Eljilany, Ella Castellano, and Ahmad A. Tarhini. *Adjuvant Therapy for High-Risk Melanoma: An In-Depth Examination of the State of the Field*. Aug. 2023. DOI: [10.3390/cancers15164125](https://doi.org/10.3390/cancers15164125).
- [6] Rebecca Lee et al. “Adjuvant therapy for stage II melanoma: the need for further studies”. In: *European Journal of Cancer* 189 (Aug. 2023). ISSN: 18790852. DOI: [10.1016/j.ejca.2023.05.003](https://doi.org/10.1016/j.ejca.2023.05.003).
- [7] Chryssoula Papageorgiou et al. “Melanoma: Staging and Follow-Up”. In: *Dermatology Practical & Conceptual* (July 2021), 2021162S. DOI: [10.5826/dpc.11s1a162s](https://doi.org/10.5826/dpc.11s1a162s).
- [8] Xiaoran Zhang et al. *Debating Sentinel Lymph Node Biopsy for Melanoma in the Modern Adjuvant Era*. Sept. 2023. DOI: [10.1200/JCO.23.00255](https://doi.org/10.1200/JCO.23.00255).
- [9] Marc Thill et al. “The Central-European SentiMag study: Sentinel lymph node biopsy with superparamagnetic iron oxide (SPIO) vs. radioisotope”. In: *Breast* 23.2 (2014), pp. 175–179. ISSN: 15323080. DOI: [10.1016/j.breast.2014.01.004](https://doi.org/10.1016/j.breast.2014.01.004).
- [10] Nushin Mirzaei et al. “Sentinel lymph node localization and staging with a low-dose of superparamagnetic iron oxide (SPIO) enhanced MRI and magnetometer in patients with cutaneous melanoma of the extremity - The MAGMEN feasibility study”. In: *European Journal of Surgical Oncology* 48.2 (Feb. 2022), pp. 326–332. ISSN: 15322157. DOI: [10.1016/j.ejso.2021.12.467](https://doi.org/10.1016/j.ejso.2021.12.467).
- [11] Michael Douek et al. “Sentinel node biopsy using a magnetic tracer versus standard technique: The SentiMAG multicentre trial”. In: *Annals of Surgical Oncology* 21.4 (2014), pp. 1237–1245. ISSN: 15344681. DOI: [10.1245/s10434-013-3379-6](https://doi.org/10.1245/s10434-013-3379-6).
- [12] *EUROPEAN PATENT APPLICATION*. Tech. rep.
- [13] Eliane R. Nieuwenhuis et al. “Performance of a Nonlinear Magnetic Handheld Probe for Intraoperative Sentinel Lymph Node Detection: A Phantom Study”. In: *Annals of Surgical Oncology* (2023). ISSN: 15344681. DOI: [10.1245/s10434-023-14166-z](https://doi.org/10.1245/s10434-023-14166-z).
- [14] Anke Christenhusz et al. *Magnetic procedure for sentinel lymph node detection and evaluation of metastases: Design and rationale of the Lowmag trial*. Tech. rep. URL: <http://www.trialregister.nl>.
- [15] Loeki Aldenhoven et al. “Sentinel lymph node mapping with superparamagnetic iron oxide for melanoma: a pilot study in healthy participants to establish an optimal MRI workflow protocol”. In: *BMC Cancer* 22.1 (Dec. 2022). ISSN: 14712407. DOI: [10.1186/s12885-022-10146-w](https://doi.org/10.1186/s12885-022-10146-w).
- [16] Kosuke Murakami et al. “Superparamagnetic iron oxide as a tracer for sentinel lymph node detection in uterine cancer: a pilot study”. In: *Scientific Reports* 10.1 (Dec. 2020). ISSN: 20452322. DOI: [10.1038/s41598-020-64926-0](https://doi.org/10.1038/s41598-020-64926-0).
- [17] Mukesh G Harisinghani et al. *Noninvasive Detection of Clinically Occult Lymph-Node Metastases in Prostate Cancer*. Tech. rep. 2003, pp. 2491–2500. URL: <http://www.nejm.org>.
- [18] Joost J. Pouw et al. “Pre-operative sentinel lymph node localization in breast cancer with superparamagnetic iron oxide MRI: The SentiMAG Multicentre Trial imaging subprotocol”. In: *British Journal of Radiology* 88.1056 (2015). ISSN: 00071285. DOI: [10.1259/bjr.20150634](https://doi.org/10.1259/bjr.20150634).
- [19] A De Lange. *Exploring and enhancing the possibilities and performance of a low-field tabletop MRI scanner*. Tech. rep. 2021.
- [20] Michael Lustig, David Donoho, and John M. Pauly. “Sparse MRI: The application of compressed sensing for rapid MR imaging”. In: *Magnetic Resonance in Medicine* 58.6 (Dec. 2007), pp. 1182–1195. ISSN: 07403194. DOI: [10.1002/mrm.21391](https://doi.org/10.1002/mrm.21391).
- [21] Sebastiaan Waanders. *Differential Magnetometry Selective magnetometry for in vivo applications Differential Magnetometry Selective magnetometry for in vivo use*. Tech. rep.
- [22] S. Waanders et al. “A handheld SPIO-based sentinel lymph node mapping device using differential magnetometry”. In: *Physics in Medicine and Biology* 61.22 (Oct. 2016), pp. 8120–8134. ISSN: 13616560. DOI: [10.1088/0031-9155/61/22/8120](https://doi.org/10.1088/0031-9155/61/22/8120).

- [23] Joseph C. McGowan. *Basic Principles of Magnetic Resonance Imaging*. Nov. 2008. DOI: [10.1016/j.nic.2008.06.004](https://doi.org/10.1016/j.nic.2008.06.004).
- [24] Yosuke Hitata et al. *HITACHI'S FAST SPIN ECHO TECHNOLOGY Efficacies in Improving Image Quality & Usability p pr ri im me eF FS SE E TECHNOLOGY*. Tech. rep.
- [25] Mathias Blasche and Christoph Forman. *Compressed Sensing-the Flowchart*. Tech. rep. URL: [www.siemens.com/magnetom-world](http://www.siemens.com/magnetom-world).
- [26] Tomoaki Harada et al. "Evaluation of lymph node metastases of breast cancer using ultrasmall superparamagnetic iron oxide-enhanced magnetic resonance imaging". In: *European Journal of Radiology* 63.3 (Sept. 2007), pp. 401–407. ISSN: 0720048X. DOI: [10.1016/j.ejrad.2007.02.010](https://doi.org/10.1016/j.ejrad.2007.02.010).
- [27] B. B. Pultrum et al. "Detection of lymph node metastases with ultrasmall super paramagnetic iron oxide (USPIO)-enhanced magnetic resonance imaging in oesophageal cancer: A feasibility study". In: *Cancer Imaging* 9.1 (Feb. 2009), pp. 19–28. ISSN: 14707330. DOI: [10.1102/1470-7330.2009.0004](https://doi.org/10.1102/1470-7330.2009.0004).
- [28] R. Walker et al. "Turbo STIR magnetic resonance imaging as a whole-body screening tool for metastases in patients with breast carcinoma: Preliminary clinical experience". In: *Journal of Magnetic Resonance Imaging* 11.4 (Apr. 2000), pp. 343–350. ISSN: 10531807. DOI: [10.1002/\(SICI\)1522-2586\(200004\)11:4<343::AID-JMRI1>3.0.CO;2-P](https://doi.org/10.1002/(SICI)1522-2586(200004)11:4<343::AID-JMRI1>3.0.CO;2-P).
- [29] Aaron T. O'Brien et al. *T2 mapping in myocardial disease: a comprehensive review*. Dec. 2022. DOI: [10.1186/s12968-022-00866-0](https://doi.org/10.1186/s12968-022-00866-0).
- [30] Eliane R. Nieuwenhuis et al. "A complete magnetic sentinel lymph node biopsy procedure in oral cancer patients: A pilot study". In: *Oral Oncology* 121 (Oct. 2021). ISSN: 18790593. DOI: [10.1016/j.oraloncology.2021.105464](https://doi.org/10.1016/j.oraloncology.2021.105464).
- [31] Andrew J Taylor et al. *T1 Mapping Basic Techniques and Clinical Applications*. Tech. rep. 2016. URL: <http://www.acc.org/jacc-journals-cme>.
- [32] S. Salamzadeh et al. "Settings of DiffMag handheld probe for maximal detection depth aiming perioperative lymph node harvesting". In: *International Journal on Magnetic Particle Imaging* 9 (2023). ISSN: 23659033. DOI: [10.18416/IJMPI.2023.2303052](https://doi.org/10.18416/IJMPI.2023.2303052).
- [33] David Moratal et al. "k-Space tutorial: An MRI educational tool for a better understanding of k-space". In: *Biomedical Imaging and Intervention Journal* 4.1 (Jan. 2008). ISSN: 18235530. DOI: [10.2349/biij.4.1.e15](https://doi.org/10.2349/biij.4.1.e15).
- [34] Jelle Veraart et al. "Gibbs ringing in diffusion MRI". In: *Magnetic Resonance in Medicine* 76.1 (July 2016), pp. 301–314. ISSN: 15222594. DOI: [10.1002/mrm.25866](https://doi.org/10.1002/mrm.25866).
- [35] Thom Van Ommeren et al. *Signal Artefacts of Moving Metal: DiffMag Handheld Probe*. Tech. rep. 2024.
- [36] Kyungsu Kim et al. "Identification of Metastatic Lymph Nodes Using Indocyanine Green Fluorescence Imaging". In: *Cancers* 15.7 (Apr. 2023). ISSN: 20726694. DOI: [10.3390/cancers15071964](https://doi.org/10.3390/cancers15071964).
- [37] Sameh H. Emile et al. *Sensitivity and specificity of indocyanine green near-infrared fluorescence imaging in detection of metastatic lymph nodes in colorectal cancer: Systematic review and meta-analysis*. Nov. 2017. DOI: [10.1002/jso.24701](https://doi.org/10.1002/jso.24701).
- [38] Nicola Rocco et al. "New techniques versus standard mapping for sentinel lymph node biopsy in breast cancer: a systematic review and meta-analysis". In: *Updates in Surgery* 75.6 (Sept. 2023), pp. 1699–1710. ISSN: 20383312. DOI: [10.1007/s13304-023-01560-1](https://doi.org/10.1007/s13304-023-01560-1).
- [39] Javier Perez Y Perez. *MELADIFF: Staging Melanoma with MRI DIXON?* Tech. rep. 2024.
- [40] K. Motomura et al. "Superparamagnetic iron oxide-enhanced MRI at 3 T for accurate axillary staging in breast cancer". In: *British Journal of Surgery* 103.1 (Jan. 2016), pp. 60–69. ISSN: 13652168. DOI: [10.1002/bjs.10040](https://doi.org/10.1002/bjs.10040).
- [41] *Ferronova*. 2024.

# A MelaDiff trial

## A.1 Summary MelaDiff protocol

Rationale: The sentinel lymph nodes (SLNs) are the first lymph nodes (LNs) to drain the tumor site and therefore the first LNs to bare metastases. Hence the importance to investigate these LNs for the best treatment strategy. Current-standard-of-care for melanoma patients with a melanoma stage of pT1b or higher, involve a surgical procedure, referred to as SLN biopsy (SLNB). The SLNB procedure involves a combined detection procedure using a radio-active tracer (Tc99-m nanocolloid) and optionally blue dye (Patent blue) followed by surgical dissection and evaluation of the LNs at the histopathology department. Due to the use of radioisotopes, this procedure suffers from several disadvantages such as limited availability, strict rules and regulations, degradation time in patient and radioactive load for user and patient.

To overcome the limitations of a radioactive tracer, a magnetic SLNB was developed which is facilitated by super paramagnetic iron-oxide (SPIO) nanoparticles. This potentially offers numerous benefits making surgery planning more flexible: no exposure to radiation, easy accessibility of the tracer, long shelf life and long half time in the patient. However, the currently available commercial product for intraoperative detection of SPIO-enhanced LNs (Sentimag®), Endomagnetics, ltd., United Kingdom) is hampered by a relatively low detection depth, biological noise, and effects of surgical equipment. With the current Sentimag® probe, the surgeons need to switch to plastic or carbon equipment and the system needs to be balanced prior to each measurement, which increases the surgery time by 20%. A new and effective way to localize SPIOs is differential magnetometry (DiffMag). This patented detection principle, developed by MD&I group at University of Twente (UT), utilizes the nonlinear magnetic response of nanoparticles. While this innovative approach has shown promising results in test environment, the DiffMag has not previously been used in clinical setting and may require further optimization. Clinical insights and feedback from healthcare professionals are essential to this ongoing refinement process.

An additional advantage of SPIOs is their visibility on MRI, which could provide mapping the SLNs preoperatively. Especially in patients with melanomas on the abdomen or back this would be very useful to see which lymph node stations are connected to the melanoma. In addition, studies have shown that SPIOs are absorbed into lymph nodes in different ways, depending on the presence of metastases. SPIOenhanced MR lymphography could therefore provide an opportunity for a non-invasive preoperative assessment of nodal status. In this pilot study we want to evaluate the clinical use of the DiffMag handheld probe for further optimization. Moreover, we want to map the lymph nodes preoperatively using MR lymphography. In addition, ex vivo MRI will be used to examine the possibility of assessing the nodal status.

### **Objective:**

#### **Primary objective:**

Assessing feasibility and usability of the handheld DiffMag magnetometer (facilitated by the magnetic tracer, Magtrace®) for localizing SLNs in melanoma patients during a SLNB procedure.

#### **Secondary objectives:**

Assessing the feasibility of LN mapping and staging with preoperative enhanced MRI enhanced by SPIONs.

**Study design:** Interventional, minimally invasive, pilot study in melanoma patients.

### **Study population:**

20 adult patients with melanoma of the upper and lower extremities, scheduled for a SLNB will be approached to participate in the study.

### **Intervention (if applicable):**

Preoperative, patients will receive two MRI-scans (optional) and a magnetic tracer injection at the primary tumor site. During surgery, SLNs will be detected using two types of magnetometers (SentiMag® & DiffMag) in addition to the standard procedure.

**Main study parameters/endpoints:** 1. SLN detection measured by DiffMag vs radioactive detection. 2. SLN detection measured by DiffMag vs SentiMag®. 3. Usability DiffMag  
**Secondary study parameters/endpoints:** 1. Usability of LN mapping by SPIO-enhanced MRI 2. Usability of LN staging by SPIO-enhanced MRI

## A.2 Approval MEC-U



Medical research Ethics  
Committees United

Postbus	Postbus 2500 3430 EM Nieuwegein
Bezoekadres	Koekoekslaan 1 te Nieuwegein 088 320 8784
E-mail	info@mec-u.nl
Website	www.mec-u.nl

Universiteit Twente  
Mevrouw A. Christenhusz MSc  
Drienerlolaan 5  
7522 NB ENSCHEDE

Betreft: besluit **R23.097**  
NL79537.000.22

Datum: 19-4-2024

Geachte mevrouw Christenhusz,

Hierbij ontvangt u het besluit van MEC-U over uw onderzoeksvorstel getiteld: "*MR lymphography and magnetic sentinel lymph node biopsy in melanoma patients measured with DiffMag*" en ons registratienummer **R23.097**.

MEC-U verleent haar goedkeuring aan het onderzoek. De goedkeuring betreft de uitvoering in de in het besluit vermelde centra.

Zie het bijgevoegde besluit voor de overwegingen bij het besluit.

Wij maken u erop attent dat *voordat* het onderzoek van start gaat, een getekend exemplaar van de goedgekeurde versie van het onderzoekscontract ter kennisgeving bij ons moet worden ingediend.

MEC-U wijst u erop dat definitieve toestemming van de Raad van Bestuur van de deelnemende centra nodig kan zijn voordat tot uitvoering van het onderzoek kan worden overgegaan.

Wij vertrouwen erop u hiermee voldoende te hebben geïnformeerd.

Met vriendelijke groet,  
secretariaat MEC-U

### A.3 Approval 'lokale uitvoerbaarheid' ZGT



Mevrouw dr. H.M. Dijkstra  
Voorzitter Raad van Bestuur

POSTADRES  
Postbus 7600  
7600 SZ Almelo

UW KENMERK	ONS KENMERK	DOORKIESNUMMER	DATUM
	ZGT24-18	06 - 23 49 31 66	03 juni 2024

ONDERWERP  
Lokaal uitvoerbaarheids advies

Geachte mevrouw Dijkstra,

In de vergadering van de Adviescommissie Lokale Uitvoerbaarheid Wetenschappelijk Onderzoek (ALU) d.d. 07 mei 2024 is de melding experimenteel onderzoek getiteld:

*'MR lymphography and magnetic sentinel lymph node biopsy in melanoma patients measured with DiffMag'*

beoordeeld. De studie zal worden uitgevoerd in ZGT. De lokale onderzoekscoördinator is mw. D. de Leeuw, chirurg.

De adviescommissie geeft een positief advies af voor de lokale uitvoerbaarheid van deze studie. **De adviescommissie heeft de volgende algemene opmerkingen m.b.t. medische hulpmiddelen:**

- **Alleen medische hulpmiddelen:**  
'Verder geldt in het algemeen dat als één van de randvoorwaarden voor toelating medische hulpmiddelen niet in akkoord is, de studie alsnog niet door kan gaan.'

In de beoordeling betrokken documenten:

- Protocol d.d. 24 mei 2022;
- Patiënteninformatie/toestemmingsverklaring, ZGT-versie oktober 2023;
- ABR-formulier d.d. februari 2024;
- Onderzoeksverklaring/studiebegroting getekend door dhr. E. Monteban d.d. april 2024;
- Verzekeringscertificaat CNA / Hardy d.d. 07 maart 2024;
- VGO deel A en B d.d. april 2024.

Vertrouwende u hiermee voldoende te hebben geïnformeerd.

Met vriendelijke groet,  
Namens de Adviescommissie Lokale Uitvoerbaarheid  
Wetenschappelijk Onderzoek,

A handwritten signature in blue ink, appearing to read 'L. Lubbers-Amsink', is written over a light blue horizontal line.

L. Lubbers-Amsink  
Secretaresse ZGT Academie

## B Lymphatic system of pigs

Figure B.1 provides a schematic overview of the lymphatic system in pigs. Pigs have two locations where lymph nodes can be detected transcutaneously: the head/neck area and the groin area. For the head/neck area this is the ventral superficial cervical LN, the middle superficial cervical LN and dorsal cervical LN. To facilitate drainage to these LNs, injections must be given in the tongue. In the groin area are the superficial inguinal LN and the superficial popliteal LN located. To drain to these areas, injections must be done in the hind limb. Other lymph nodes are situated deeper and can be reached by surgically opening the pig and extracting abdominal organs.

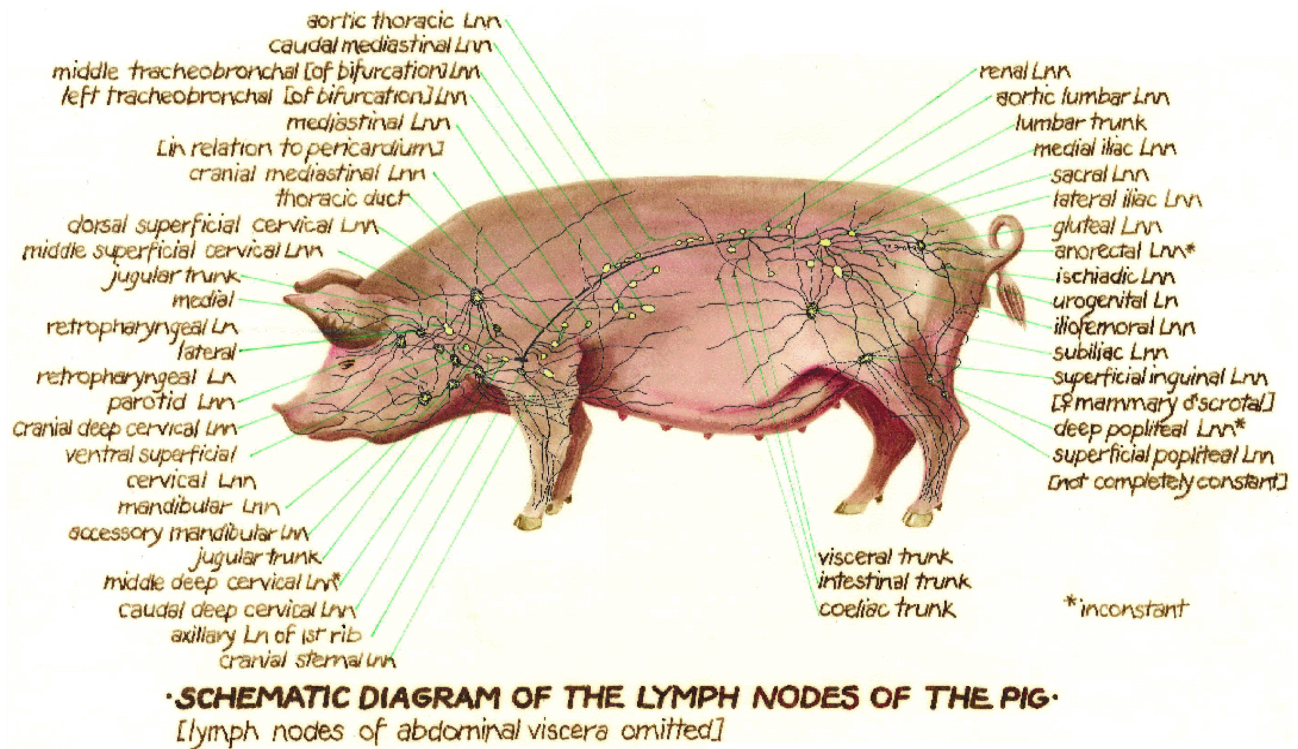


Figure B.1: Schematic overview of lymphatic system of pigs[41]

## C Questionnaire usability DiffMag handheld probe

### Questionnaire usability DiffMag

The questionnaire is based upon a standardized questionnaire for assessing perceived usability, the system usability scale[39]. We have adapted this scale to fit our needs in perceiving usability from surgical and cleaning perspective.

Surgeon: Technical Medicine student: Iris Huinink  
 Date of surgery: Surgery on in vivo porcine model: 28-02-2024  
 Product Specialist:  
 Patient Number:

	Strongly disagree				Strongly agree
	1	2	3	4	5
1. I think that I would like to use this system frequently.				X	
2. I found the system unnecessarily complex.		X			
3. I thought the system was easy to use.				X	
4. I think that I would need the support of a technical person to be able to use this system.		X			
5. I found the various functions in this system were well integrated.				X	
6. I observed a notable inconsistency in this system, concerning interference with metal.				X	
7. I would imagine that most people would learn to use this system very quickly.					X
8. I found the system very cumbersome to use.	X				
9. I felt very confident using the system.				X	
10. I needed to learn a lot of things before I could get going with this system.	X				
11. I found it easy to disinfect the system.					X

→ Only when surgical instruments were close to the probe